On the relationship between water vapour field evolution and the life cycle of precipitation systems

Joël van Baelen, M. Reverdy, F. Tridon, L. Labbouz, G. Dick, M. Bender, M. Hagen

Quarterly Journal of the
Royal Meteorological Society

On the relationship between water vapour field evolution and precipitation systems lifecycle

Journal:	*QJRMS*
Manuscript ID:	QJ-10-0070.R2
Wiley - Manuscript type:	Research Article
Date Submitted by the Author:	n/a

Complete List of Authors:	Van Baelen, Joel; LaMP / OPGC Reverdy, Mathieu; LaMP/OPGC Labbouz, Laurent; LaMP/OPGC Tridon, Frédéric; LaMP/CNRS Dick, Galina; Helmholtz Centre Potsdam, German Research Centre for Geosciences Bender, Michael; Helmholtz Centre Potsdam Hagen, Martin; DLR

Keywords:	water vapour, GPS tomography, precipitation systems, convective initiation, weather radars

On the relationship between water vapour field evolution and Precipitation systems lifecycle

Van Baelen[1*] J., M. Reverdy[1], F. Tridon[1], L.Labbouz[1],

G. Dick[2], M. Bender[2], and M.Hagen[3]

1) Laboratoire de Météorologie Physique, CNRS – University Blaise Pascal, Clermont-Fd, France

2) Helmholtz-Centre Potsdam, GFZ, German Research Center for Geosciences, Potsdam, Germany

3) Deutsches Zentrum für Luft- und Raumfahrt (DLR), Oberpfaffenhofen, Germany

Manuscript prepared for the COPS special issue of the

Quarterly Journal of the Royal Meteorological Society

31 October 2010

Corresponding author address:

LaMP, Université Blaise Pascal, 24 Avenue des Landais, P.O. Box 80026, 63171 Aubière CEDEX, France

E-mail : j.vanbaelen@opgc.univ-bpclermont.fr

Abstract

In this work, we investigate the relationship that can be found between precipitation systems structure and evolution, from initiation to decay, and the associated water vapour field distribution during the COPS (Convective Orographically-induced Precipitation Study) international field campaign which took place from the Vosges to the Black Forest Mountains, across the Rhine Valley, in summer 2007. In particular, we consider water vapour retrieval through GPS Integrated Water Vapour 2-D maps as well as 3-D tomography and confront it to precipitation systems observed with the ground based C band POLDIRAD weather radar.

On one hand, we have evidenced the predominant role of water vapour as a precursor to convective initiation for local convective cell generation. Water vapour accumulation on the crest of the orography is associated with ridge convection, while water vapour passing over the mountain top and creating valley outflows generates lee side convection often triggered by a small hill positioned within or close to the valley exit, or by a local convergence with the plain water vapour field.

On the other hand, we have noted that frontal systems seemed to develop preferably where the largest amount of water vapour was available. Likewise, in the case of frontal systems, well formed synoptic scale storms are associated with high water vapour signatures, while lighter systems with embedded convection appear to trail high water vapour areas where the convective part is associated with local water vapour depletion. This later aspect could be the signature of the convective cloud formation, when water vapour is transferred into liquid water, before the onset of precipitation.

I/ Introduction

The COPS (Convective Orographically-induced Precipitation Study) international field campaign took place in the summer of 2007 from June to August, in the region of South-West Germany / North-East France, across the Rhine Valley from the Vosges Mountains to the Black Forest Mountains (Figure 1). The overall objective of COPS is to improve the Quantitative Precipitation Forecast (QPF) skill of Numerical Weather Prediction (NWP) models over mid-range mountainous terrain. Hence, the research interests of the campaign deal primarily with the study of the meteorological conditions and forcing mechanisms leading to convective initiation, with the monitoring of the precipitation life cycle, and with the analysis of the role played by orography on initiation and development of the precipitation system. To achieve this goal, a large set of in-situ and remote sensing instrumentation was deployed over a series of super sites at selected locations across the domain of interest, while numerous operational and research models were run operationally to assess their performances with respect to the different events observed during Intensive Operation Periods (IOP's).

For more details on the campaign background, on its implication within other international efforts, on the strategy of the observations and campaign implementation, on the description and characteristics of the instruments deployed, and on some preliminary results, please see Wulfmeyer et al. (2008) and Wulfmeyer et al. (2011). Likewise, reports on results and ongoing research in the framework of COPS can be found in Kottmeier et al. (2008) and in the various papers of this special issue.

The scientific scope of the present paper only tackles a small aspect of this ambitious program. It focuses on the preliminary investigation of the relationship that can be found between the

precipitation system structure, intensity and dynamics, from initiation to decay, and the associated water vapour field distribution and evolution. In particular, we will consider water vapour retrieval exclusively through GPS tomography and precipitation systems monitoring with ground based radars only. At this point we easily acknowledge that this provides only a partial view of the problem, while further investigations using increased resolution and other means of measurements are still in progress. Nonetheless, the underlying questions of the current work deal with the role of water vapour as a precursor and/or tracer of precipitation activity, with the effect of orography on the water vapour field distribution and evolution, with the necessity (or not?) of water vapour convergence to start convective activity or foster precipitation system enhancement, etc. but also with the capability of the GPS tomography to provide an adequate tool to study such problems.

In section 2, we will present the experimental set-up deployed during the COPS campaign that provided the data we have used in this study: the GPS network, the POLDIRAD (Polarimetric Diversity Doppler Radar) C- band (~5 GHz) research radar and the French super-site UHF (~1.2 GHz) wind profiler. In section 3, we will describe the GPS signal processing as well as the tomography algorithm used and discuss its scope and current limitations. In section 4, we will focus on particular IOP cases where precipitation events were monitored with POLDIRAD to study their associated GPS retrieved water vapour field and its evolution before and during the rain. Finally, in section 5, we will offer some preliminary conclusions and comments, and outline further work and developments.

II/ The experimental set-up

For more than a decade, the GPS (Global Positioning System) has proven to be an autonomous, all-weather and continuous system for the restitution of the atmospheric water vapour (Bevis et al., 1992; 1994; Businger et al., 1996). With such a technique, one can retrieve the IWV (Integrated Water Vapour) representative of the atmospheric column above the GPS station with good accuracy (Tregoning et al., 1998; Van Baelen et al., 2005; Wang et al., 2007). Furthermore, when a dense network of GPS stations exists, GPS can be used to perform tomography in order to retrieve the three dimensional distribution of water vapour density (Flores et al, 2000; 2001; Gradinarsky and Jarlemark, 2004; Champollion et al., 2005; Reverdy et al., 2009).

Therefore, as part of the COPS instrumental set-up, the existing networks of GPS stations in France and Germany were enhanced with temporary stations such that an average separation of less than 40 kilometres between GPS stations over the entire COPS domain was achieved. Furthermore, a denser segment of stations separated by about 10 kilometres was also created from the crest of the Vosges to the Black Forest, across the Rhine valley. This segment was somewhat aligned with the different supersites of the campaign. Figure 1 shows the resulting network of GPS stations that provided data for the present work. The stations within the network have distributed altitudes, some installed in the plains or valleys, others implemented on the mountains to offer a homogenous representation of the varying terrain of the region. Within the network, most stations stand between 136 m ASL and 912 m ASL (with the exception of the station installed at the Hornisgrinde supersite at 1213 m ASL). For all GPS stations, data were recorded with a 30 second sampling interval and an elevation cut-off angle of 5°.

In order to relate on the water vapour field evolution and patterns retrieved through GPS tomography to the different characteristics of precipitating systems, we use weather radar

observations to monitor the convective initiation, the onset of precipitation and the subsequent development of those precipitation systems.

The polarimetric C-band Doppler research radar POLDIRAD (Schroth et al., 1988) of DLR (Deutsches Zentrum für Luft- und Raumfahrt) was deployed for 3 months in the foothills of the Vosges Mountains at Waltenheim-sur-Zorn at 260 m MSL, about 20 km north-west of Strasbourg. Its location was about 100 m above the floor of the Rhine Valley providing an undisturbed overview over the Rhine Valley, the Black Forest and the Vosges in order to ideally complement the existing operational weather radars from Deutscher Wetterdienst, MeteoFrance and MeteoSwiss. During IOPs, volume PPI (Plan Position Indicator) scans were performed up to 120 km range every 10 to 20 minutes.

For the COPS campaign, the Vosges supersite also included a UHF boundary layer wind profiler fielded by the CNRM (Centre National de Recherches Météorologiques) of Meteo France in the plains a few kilometres east of the Vosges foothills (Richard et al., 2009). This radar provides vertical profiles of wind amplitude and direction with 75 m height resolution from 150 m above the ground up to about 3 km and with a 15 minute time resolution in its high resolution mode. However, this wind profiler was only deployed during the month of July.

Figure 1 indicates the locations of the POLDIRAD radar and of the French super-site, where the UHF radar was installed.

III/ GPS processing and tomography for water vapour field retrieval

The GPS data collected throughout the campaign were processed with the EPOS (Earth Parameter and Orbit System) software package developed at the GFZ (GeoForschungZentrum, Potsdam, Germany) (see Gendt et al., 2001, 2004 for detailed description of EPOS). Globally, the EPOS software can estimate different parameters from GPS observations. It can be used for various applications by configuring the processing correspondingly, for example IGS (International GNSS Service) data processing, GPS campaign and GPS meteorology. For GPS meteorological applications, data can be processed in network mode and Precise Point Positioning (PPP) mode (Zumberge et al., 1997) with the EPOS software. In PPP mode, all satellite related parameters, i. e. satellite orbits and clocks, earth rotation parameters, etc. are assumed to be well known, so that there are no common parameter among stations, consequently the data can be processed station by station, i.e. in PPP mode. This enables data of a larger number of GPS stations observed simultaneously, for example, data from a dense network, to be processed independently on different processors and/or computers. In order to obtain the satellite related parameters, a global network should be processed in the similar way as for the generation of the IGS ultra-rapid or rapid products which can usually only be carried out by IGS Analysis Centres like GFZ. Here for regional GPS meteorological applications, to involve some stations around the network will improve the parameters needed to be fixed in PPP data processing. EPOS is based on a least-squares adjustment of zero-differenced phase and range observations. The advantage of using zero-differenced observations is that ray path residuals required to construct the slant total delays (STDs) are available directly in form of observation residuals.

For precise positioning the signal delay due to the neutral atmosphere needs to be modelled. The zenith total delay (ZTD) and atmospheric gradients in NS and EW direction are therefore estimated together with the geodetic parameters. The STD along a given signal path can be approximated by applying the Global Mapping Function (GMF) (Boehm et al., 2006) or the Niell

mapping function (Niell, 1996) to the ZTDs while the horizontal atmospheric inhomogeneity is provided by the gradients. Hence, contributions to the path delay which cannot be described by this model go into the ray path residuals. To obtain more precise atmospheric parameters the station coordinates and several other parameters are fixed in the troposphere PPP run. Due to the reduced number of free parameters the residuals are dominated by unmodelled atmospheric contributions while the impact of other uncertainties is minimised. Under these assumptions the STD is given by

$$STD = m_h \cdot ZHD + m_w \cdot [ZWD + \cot \varepsilon \, (G_N \cos \varphi\_ + G_E \sin \varphi \, \_)] + \delta$$

where the *ZHD* and *ZWD* are the hydrostatic and the wet zenith delay, respectively, m_h and m_w are the hydrostatic and the wet mapping functions, G_N and G_E are the delay gradient parameters in the northern and eastern direction, ε is the elevation, φ is the geographic latitude and δ is the post-fit phase residual. In this automated signal analysis, the hydrostatic and the wet contributions to the ZTD are separated using the Saastamoinen model and climatological data. The zenith delays and mapping functions alone lead to STDs which are rotationally symmetric. The information about spatial atmospheric structures is mainly provided by the residuals _ and to a minor degree by the gradients.

The errors of the GPS observations and the rather complicated processing chain are difficult to estimate. Therefore, it is important to validate the ZTD and STD estimates with independent observations (Duan et al., 1996; Ware et al., 1997; Liljegren et al., 1999; Braun et al., 2003, Van Baelen et al., 2005) or models (Ha et al., 2003; Liu et al., 2006). Inter-comparison studies with water vapour radiometers and weather models show a STD bias below 1 mm for elevations greater than 30° and below 1.5 mm for elevations down to 5° (Bender et al., 2008).

For meteorological applications the availability and the temporal resolution of these data is important. Currently, GPS raw observations with a sampling rate of 2.5 minutes are processed on a hourly basis and the results are available in near real-time. A 12 hour sliding window with 1 h steps is used to process the tropospheric parameters for the most recent hour. Gradients are estimated once per hour, ZTDs for 15 minutes intervals. STDs are retrieved with the full sampling rate of 2.5 minutes by adjusting the corresponding residuals for each individual satellite-receiver link. 96 ZTDs and about 4500 STDs are available per station and day.

For case studies, when an ensemble of GPS stations is available over a limited area, the transmission rays from satellites to receivers can interleave together and tomography inversion will allow the restitution of the three dimensional distribution of the atmospheric water vapour. Indeed, if one defines the volume above the GPS network as an ensemble of atmospheric boxes, called voxels, these voxels will be traversed by the various individual rays. Hence, in this case, the STD's are the GPS observable used for tomography but, first, they have to be converted into SIWVs (Slant Integrated Water Vapour) which correspond to the humidity induced part of the tropospheric delay in the propagation from the satellite to the receiver. To derive the SIWVs from the STDs, one has first to subtract the corresponding hydrostatic part. For precise meteorological analysis, that step requires to determine the pressure field, determined from meteorological surface stations for example, and to calculate the hydrostatic component along each ray, using Saastamoinen's formulation (1972), as it propagates through the atmospheric volume above the analysis domain. Then, following relations defined by Emardson and Dirks (1999) that make use of the atmospheric temperature, the resulting SWD (Slant Wet Delay) can be converted into SIWV. Once these SIWV are determined, they are distributed among the different voxels of the analysis domain, according to the length of their path within each voxel

they cross and weighted by the vertical distribution of the standard atmosphere (i.e., more weight to the lower levels where water vapour is more abundant). These lengths are essential to create the linear operator of the tomography. Also, we consider that there is no water vapour above an altitude of 12km. Likewise, when one of the ray quits the analysis domain through one of the side limits of the analysis domain, under 12 kilometres of altitude, it is accounted for only its proportional path within the domain as SIWV are integrated values.

Depending on the GPS station and satellite geometry, some voxels will contain data (one or multiple rays), especially in the highest layers of the atmosphere, while some others might not, in particular in the lowest layers of the grid. Thus, we face a partially determined problem that can be written under the following equation [Tarantola, 2005]:

$$d = G \times m$$

where d represents the data (SIWV), G the model we will use, i.e the linear operator providing the length distribution of SIWV through the voxels and m corresponds to our results, i.e., the water vapour density distribution in the voxels. A solution to that linear problem is given by a weighted least square fit equation solution (Menke, 1989; Tarantola, 2005):

$$m^{est} = m_0 + \left(G^t \times W_{GPS} \times G + \alpha^2 \times W_{Model}\right)^{-1} \times G^t \times W_{GPS} \times \left(d - G \times m_0\right)$$

where m_0 is an a priori solution or first guest, W_{GPS} corresponds to the inverse of the variance/covariance matrix of the data errors : $W_{GPS} = \left(C_{GPS}\right)^{-1}$, W_{Model} corresponds to the matrix of the variability of the model around the a priori values, G is the model, and α is a weighting

coefficient. In theory, by varying α, one can vary the respective weight on the data or on the a priori estimation. The larger the α, the more weight is given to the initialization as a solution and, inversely, the lesser the α, the more weight is given to the data. The influence of α is still the object of ongoing sensitivity work, so we have chosen here a solution akin of a regular least square fit equation by keeping α neutral, i.e. equal to 1. Further details are provided in (Reverdy, 2008).

Hence, another important step in the tomography inversion process is to initialize the inversion matrix, i.e. provide an "*a priori*" solution. In our case, this is done with a standard atmosphere profile, i.e., an exponentially decreasing profile with altitude (McClatchey et al., 1972), adjusted to the voxel column IWV derived from the GPS measurements. First, the GPS derived IWV field is interpolated through out the analysis domain. Then, for each voxel column, the corresponding mean IWV and mean topography are computed. Finally, the standard profile contribution above the equivalent altitude is scaled to match the mean GPS derived IWV and reported in the a priory solution for the corresponding voxel column. Thus, for the tomography that we have developed and implemented here, we rely uniquely on the GPS observables although making use of outside sources of information such as radiosondes (Champollion et al., 2009), microwave profiling radiometers (MacDonald et al., 2002) or even lidar measurements could easily be adapted and will be the object of future work. However, it has been our choice also to restrict the GPS tomography by not using external water vapour profiles for two reasons: first, we wanted to avoid reducing tomography to merely filling the time steps between successive profiles interpolations although we know we will lack vertical structure reconstruction when the spacing between GPS stations is too large, and second, the profiles "assimilation" strategies can have a significant influence on the resulting fields and we wanted to see how much could be extracted from GPS alone.

Once the water vapour field is initialized and the SIWV have been adequately distributed among the corresponding voxels, then the tomography resolution is a mere weighted least square equation inversion problem (Reverdy, 2008) where the resulting matrix is the 3-D distribution of water vapour density in the various voxel defined over the analysis domain.

In the case studies presented hereafter, the basic tomography was run with a 14 x 14 x 16 voxel grid covering the COPS area from 47.5° North to 49.5° North and from 6.25° East to 9.25° East, corresponding to a 16 km horizontal resolution with a varying height resolution getting coarser with altitude as water vapour amounts decreases, starting at 500 m height resolution up to 4 km of altitude, increasing to 750 m height resolution up to 7 km of altitude and finally ending at 1000m height resolution up to the maximum analysis height of 12 km of altitude where the water vapour is deemed negligible, and using all of the GPS station data available for the domain shown in Figure 1. For increased resolution and to avoid artefacts due to lack of information brought by excessive spacing between GPS stations, we have also run the tomography analysis on a sub section of the domain where the GPS station density was the largest, from 48.0° North to 48.9° North and from 6.7° East to 8.5° East, with a 12x12x16 voxel grid for an horizontal resolution of about 10 km (8.4 km x 11.2 km) and an unchanged vertical resolution of 500 m in the lower levels.

IV/ Case studies and discussion

In this paper, we have taken the approach to use exclusively GPS IWV fields and tomography water vapour retrieval in conjunction with local radar observations to consider the precipitation systems behaviour. Hence, the case studies will necessarily be limited in their scope as numerous

atmospheric parameters, such as those derived from radiosondes (Convective Available Potential Energy - CAPE, Convective Inhibition - CIN, Richardson number, etc.) or also VERA (Vienna Enhanced Resolution Analysis) (Steinacker et al., 2006) for low level dynamics for example, are not used or accounted for at this time.

Therefore, in these preliminary investigations, we aim at providing only a broad ensemble description of the processes involved rather than a detailed analysis of a single event. This descriptive approach is also dictated by some of the current physical limitations of tomography regarding its application to this work. Indeed, with simple geometrical considerations based on the tomographic resolution (the size of the voxels) and the spacing between the network GPS stations (about double the voxel size on average), one can easily recognize that there will be a significant number of empty voxels, i.e. voxels without a ray crossing it. That is especially true at the lower levels as rays from a given station will most probably stay within the boundaries of the first altitude level voxel above it, even with a 5° elevation mask. On the first altitude level, in the current geometry, about two thirds of the voxels are empty. Furthermore, at the levels just above, few voxels will be traversed by rays from different stations. These limitations make for a strongly undetermined problem regarding the tomography inversion and could question the benefits of tomography with respect to simple IWV 2-D maps or its impact on the final water vapour field compared to the a-priori values. Furthermore, in those parts of the domain where there are very few GPS stations, such increased separation between stations can lead to artefacts due to the IWV interpolation in an area of contrasted topography such as, for example, in the south east border of our larger domain. However, when spacing between stations becomes less than the voxel size, at it is the case in the central part of the COPS domain (Figure 1), these restrictions are eased and the tomography inversion offers new insights into the water vapour field distribution and evolution. That is also why we have focussed our analysis on a smaller

network with enhanced resolution whenever the meteorological situation of interest happened to take place within the region of denser GPS station locations. Hence, the major obstacle in this work has come from the uneven spacing between GPS stations within the network. Statistical comparisons between a-priori and tomography water vapour fields over the entire data set have shown that although there were little differences in those areas with few GPS stations as in the S-E and W-N-W parts of the domain, variations up to 10% of the retrieved water vapour density could be found in the central part of the domain where the campaign super sites were located, surrounded by the denser part of the GPS network. Likewise, comparisons of tomography results with 2-D IWV maps have shown that although they were globally similar, some noticeable differences could be seen especially in the areas of marked contrasts like front boundaries and high gradient situations as the tomography is more apt to retrieve the anisotropy of the water vapour distribution within the denser GPS part of the domain.

The basic question we want to address in this work is the possible link that relates particular water vapour patterns with the different types of convective initiation mechanisms and precipitation system characteristics encountered during COPS. To do so , we have based our case studies selection and partitioning on the general classification provided by Wulfmeyer et al. (2011) and Kottmeir et al. (2008): 1/ High pressure air mass convection leading to locally initiated convection; 2/ Forced wide spread convection favoured by large scale lifting and orographic effects; 3/ Forced convection embedded in frontal or convergence zones. However, using radar observations, we can also use the differentiation established by Hagen et al (2011) where convection initiation takes place either 1/ on the mountain Ridges or 2/ on the Lee side of the mountains.

IV.1. IOP 8b, 15 July 2007

This first case is certainly the most studied one among the many COPS IOPs recorded. Thus, we won't duplicate the detailed observation analyses and modelling presentations already made in Kottmeir et al. (2008), as well as in Wulfmeyer et al. (2011), Bartlhott et al. (2011), Behrendt et al. (2011), and Richard et al. (2011) in this issue, and the list is certainly not exhaustive.

As shown on the radar reflectivity display of Figure 2, this event was characterized by a single isolated short lived small but very intense convective cell that developed on the eastern ridges of the Black Forest and qualifies for a "Ridge" – "High pressure air mass convection" classification. On the POLDIRAD images it is interesting to notice how the system initiates, grows, and develops through its entire life cycle with little advection, like a plume defined by a typical downstream V shape and attached to a well localized hotspot.

In Figure 3a, we show the IWV 2-D field (left column) and the horizontal water vapour density for the 1000 m height layer (right column) both for the hourly time frames from 13 to 15 UTC. Looking at these water vapour field distributions, we have to keep in mind that this might not be the best GPS analysis conditions for tomography as that area does not lie within the denser part of the GPS network, even though there is one GPS station not far away of the active cell area depicted by the black circle. Also, given that the resolution of the water vapour tomography is of the order of 16 kilometres, there is little hope to identify the hotspot where convection is activated but we can look at the larger scale evolution. In the early afternoon, a build up of humidity over the Southern Black Forest ridges is clearly visible, possibly provided by the South-Westerly flow (Wulfmeyer et al., 2011; Richard et al., 2011). However, between 13:00 UTC and 15:00 UTC, the water vapour field appears to decrease in the area where the convective cell (around 48.2°N and 8.3°E) later developed. Hence, water vapour depletion started more than

one hour before the onset of the precipitations. Comparing the tomography result to the IWV field, it is interesting to note that tomography provide a better visual description of the local variation of water vapour, although one must argue tat IWV is impacted by the topography and that its relative variation with respect to a daily mean or some reference field value would also exhibit similar build up and decrease of humidity. This fact seems to indicate that in that area, maybe due to local forcing triggered by a localized singularity in the orography or in the ground coverage or vegetation, there is a transfer from water vapour to liquid water. Indeed, GPS measures water vapour content of the atmosphere but is not sensitive to liquid (or solid) water (Solheim et al., 1999). This transfer implies the creation and/or enhancement of clouds by generation of hydrometeors through condensation first but may be also through washing of the lower atmosphere once the rain has started to fall. Such an effect of water vapour depletion to support cloud formation before heavy precipitation onset had already be considered in Van Baelen and Penide (2009) but the COPS experiment offers the first opportunity to actually observe both the 3-D water vapour field and the precipitation system development simultaneously. Further evidence is provided by the individual time series of IWV corresponding to the four GPS stations surrounding the location of convective precipitation activity (Figure 3b). Indeed, one can see the north-eastward progression of a peak of humidity within the couple of hours before noon brought by the synoptic flow (which also cleared away a pool of humidity that stagnated in the plain to the South-East of the Black forest in the morning). Then, by 12:00 UTC, water vapour starts decreasing significantly, indicating the possible condensation process, while water vapour reaches its minimum at the time the precipitation occurs.

IV.2. IOP 9c, 20 July 2007

This case is an example of forced convection embedded in a frontal zone characterized by high water vapour densities moving ahead of the front. In the scope of this paper, it serves as a support to illustrate two interesting interactions between water vapour field and precipitation systems. But again, given that the GPS station density across the event analyzed is not homogeneous, we will consider both IWV fields and tomography results.

First, in Figure 4, when comparing the POLDIRAD 10:00 UTC reflectivity plot with the integrated water vapour distribution retrieved at the same period, one can't help noticing the excellent correlation that exists between the line of active cells (the high reflectivity centres in red) within the front (the area of moderate reflectivity values in green) and the areas of water vapour depletion within the water vapour pattern. Those areas are highlighted by a white arc on the corresponding figures and exhibit a deficit of more than 6 mm (up to 15%) of integrated water vapour. Such differences are significantly larger than the recognized accuracy of GPS water vapour retrievals. Hence, this point further demonstrates the possible transfer from water vapour into liquid water (hydrometeors) in the areas of active convection, while further depletion might be produced by aggregation of the atmospheric water vapour by the hydrometeors as they drop to the ground.

Second, considering now the water vapour distribution at 10:00 UTC at the 1000 m level and the POLDIRAD 10:30 UTC reflectivity map, it appears that the frontal line development is favoured in those places where there exists enhanced water vapour "reservoirs". In this instance, that is particularly visible for the area just east of the North-East tip of France (about 48.8° N – 8.5°E), while tomography also reveals the area on the lee of the Vosges at the south end of the precipitation system Nonetheless, this figure also illustrates a current limitation with tomography in those regions with few GPS stations as artefacts can appear and mask actual water vapour

signature as this is the case here over the southern Black Forest mountains. Hence, this indicates that pre-existing water vapour conditions play a dominant role in frontal development.

IV.3. IOP 9a, 18 July 2007

We selected this case because of the very localized convection spots that could be observed with POLDIRAD. Referring to the proposed classifications, this is also a case of convective activity favoured by large scale lifting due to strong flow aloft and creating isolated cells. Obviously, this is also a case of Lee side convection as all the cells observed develop on the eastern side of the Vosges. Figure 5 presents some examples of the convective and precipitation activity observed with POLDIRAD. The first one (17:00 and 17:30 UTC time frames) takes place at the exit of the Bruche valley. There, the radar reveals that the convection is triggered by a small hill within the valley exit range. Likewise, the 18:22 – 18:54 UTC cell to the south of the Vosges super-site is also triggered by a hill at the foot of the mountain range close to the exit of the Giessen valley.

In these instances and in contrast with the July 15 case studied above, the water vapour density does not build up on top of the mountain orography but it appears to cross the ridges and flow down the lee side of the Vosges into its deepest valleys. That is well indicated in Figure 6a where the water density horizontal fields at the 1000m altitude level from 14:00 to 19:00 UTC illustrate the water vapour outflow that takes place at the outcome of the Vosges mountain valleys before continuing across the Rhine valley. First (15:00 – 16:00 UTC), it is located at the exit of the Bruche valley, then, the water vapour comes across the southern lee side of the Vosges range and, in particular, around the Giessen valley (17:00 - 18:00 UTC). On Figure 6b, paying close attention to the 7.4° E zone on the constant latitude vertical cross-sections provided at 48.65°N (Bruche valley) and 48.16°N (Giessen valley), one can see the marked water vapour density reinforcement in the lowest level, while little accumulation occurs on the west side of the

mountains ranges nor on their ridges as the water vapour crosses the Vosges and spread across the Rhine valley.

Hence, one can consider that the strong flow aloft is responsible for the water vapour crossing over the mountain ridges and not accumulating over the mountain tops. Accordingly, the GPS tomography retrieved water vapour fields indicate that it is the moist air descending from the crests into the valleys that triggers the convection initiation when the flow hits a hill at the exit of the valley which creates abrupt lifting of the low level air mass.

Furthermore, taking the opportunity of the UHF boundary layer wind profiler operation at the nearby Vosges supersite (Figure 7), one can see that during the corresponding time period between 16:00 and 18:00 UTC, the wind field is characterized by westerly flow aloft (above 1.5 km of altitude) but easterly, upslope winds in the lowest 500 m of the troposphere, causing low level convergence along the Vosges lee side. Thus, we can speculate that the outgoing flow from the valleys is meeting such upslope wind coming from the Rhine, further enhancing the lifting effect of hills positioned near the exit of those valleys and, thus, enabling convective initiation.

IV.4. IOP 15, 12 – 13 August 2007

IOP 15 is of particular interest as in the course of two days three separate case studies occur. First, there is "Ridge" convection on the 12th of August afternoon, mainly on the Vosges, followed by a frontal passage in the Rhine valley in the early hours of the night, before "Lee side" convection takes place on the 13th of August afternoon. Extensive work on the convective activity observed with radars and on the role of the wind field in the convection forcing mechanisms has already been developed in Hagen et al. (2011, this issue) and, to a lesser extend in Bennet et al (2011, this issue) and Planche et al. (2010), so here we will keep our focus on the water vapour fields / convective and precipitating systems interactions.

Figure 8 shows a series of radar observations of the "Ridge" event on the 12th of August. POLDIRAD reveals the large scale extent of the isolated cell development over the Vosges crests. Also, cell track origins (Hagen et al., 2011) for the entire episode show that the convection initiation process is confined to the ridges while their relatively small extent, with most cells decaying as they reach the Rhine valley, indicates that the advection is weak and that there must be little moisture available over the plains to fuel the convection process. The associated water vapour field distribution estimated with GPS tomography (Figure 9a and 9b) further confirms that there is accumulation of water vapour from mid-morning up to early afternoon over the Vosges Mountains to support the localized convection. In particular, the constant latitude vertical cross-sections at 48.41°N and 48.19°N between12:00 and 14:00 UTC and 13:00 and 15:00 UTC respectively, passing through very active areas of the Vosges convective zones clearly show that the water vapour does not cross the main Vosges ridge but accumulates over the crests.

During the following night, there is a frontal passage with sustained precipitations that are well documented with POLDIRAD as illustrated in Figure 10. This case can be considered as forced convection embedded within a (cold) frontal zone. In this instance; the corresponding water vapour field exhibits somewhat different behaviour from the previous discussions regarding the July 15 and July 20 cases. Indeed, it appears here that the rain activity is already well established when the system enters the COPS domain with a strong and active front brought by large scale synoptic forcing. Hence, we have no indication regarding possible transfer of water vapour into liquid water to support the creation and development of clouds and the precipitation onset, associated with water vapour depletion. Instead, we notice that in the first illustration (21:00 UTC) the precipitation system contour is well correlated with a zone of high water vapour density immediately positioned under it denoting the saturation of the atmosphere in humidity

associated with the frontal system. However, later on, high water vapour density ramifications appear to extend ahead of the frontal system depicting possible storm outflow activities such as those reported by Collier et al. (2008). Finally, considering the latest time frame (00:00 UTC on 13th of August), there is evidence of interaction of the orography with the development of the frontal system as water vapour propagation is stopped by and accumulates against the foothills of the Black Forest before rounding it by its northern tip.

Later in the afternoon of the 13th of August, well after the frontal passage is gone, a new episode of isolated convection takes place but this time it happens on the Lee of the Vosges. That is shown with the POLDIRAD observations of Figure 11, where individual cell formations can be monitored. The reported locations of the different convection initiation spots on the lee side of the Vosges (almost exclusively) and the corresponding duration of the cell tracks extending well across the Rhine valley offer a quite different pattern from the 12th of August situation (see Hagen et al., 2011 for further details). Considering now the corresponding water vapour density fields, the horizontal distribution at the 1000 m level, shown in Figure 12a, indicates no specific accumulation towards the mountain ridges but relatively high water vapour values in the Rhine valley instead and reinforcement of the water vapour density at the foothill of the Vosges in those areas and times when convection seen with POLDIRAD happen. That is the case at 12:00 and 13:00 UTC along the North-East side of the Vosges orography. Furthermore, by 15:00 and 16:00 UTC, there is a marked increase of water vapour at the exit of one of the central Vosges mountain valleys, associated with the generation of a strong cell identified in the South of the POLDIRAD field of view at 16:30. To better illustrate these findings, Figure 12b shows two series of vertical cross sections at constant latitude. The first one at 48.19°N spans the time range from 12:00 to 14:00 UTC and passes through the cells observed on the North of the Vosges mountain range. Besides, high values of water vapour in the Rhine valley and along the western

slopes of the Black Forest, it shows a local burst of water vapour at the foot of the Vosges Mountains at 13:00 UTC, corresponding to the precipitation cells monitored. Likewise, the second series of vertical cross sections at constant latitude 48.41°N spans the time range from 15:00 to 17:00 UTC and passes through the cell observed in the southern domain of POLDIRAD in Figure 11. In this case, the strong water vapour outflow associated with the convective cell initiation corresponds to water vapour advection above the mountain ridge onto the lee side down along mountain valley. Also quite interesting is Figure 12c, where we present the vertical cross sections at constant longitude spanning the time range from 11:00 to 16:00 UTC and passing along the Vosges front ranges. Looking at the first three time frames (11:00 to 13:00 UTC), we find a strong evidence of water vapour convergence at the location of a small hill by about 48.5°N where the strong cell visible at 13:00 with POLDIRAD develops. Indeed, from 11:00 to 12:00, water vapour levels increase significantly on both sides of the central hill but by 13:00, water vapour has now converged on that hill where convective initiation takes place. Later, the strong outflow leading to the large convective cell initiation in the south of POLDIRAD field of view is also well identified with a major increase of water vapour density over the first levels of the atmosphere around the 48° N latitude.

V/ Concluding remarks and future work

In this work, we have considered the water vapour field evolution with respect to the various precipitation and convective initiation situations monitored during the COPS campaign. Hence, we have tried to gain new insights on the role of water vapour in the precipitation systems lifecycle. To do so, we have looked at the water vapour field patterns and behaviour as a function

of orography dependant convective initiation, i.e. Ridge or Lee side convection, as well as a function of background synoptic conditions for larger scale systems.

First, for ridge convection, it is necessary to get significant water vapour accumulation over the crests of the mountains as a precursor to convection onset. That implies that the synoptic wind is not too important such that it does not carry the water vapour across the range, or that local conditions or singular orographic features favour water vapour blocking and accumulation over the crest. Then, the water vapour acts as a fuel for the convective initiation or regeneration over the mountain ridge. On the opposite, when the water vapour does not stagnate over the mountains but passes the ridge to flow down the main orography, the corresponding valley flows are prone to generate lee side convection when they encounter a small hill and/or some converging flow coming from the wormer plains in the lowest layers of the atmosphere. This combined effect probably creates a significant lifting of high water vapour air and triggers convection.

Second, we have noticed an interesting feature where water vapour seemed to decrease singularly some times before the actual onset of precipitation or precipitation reinforcement. One hypothesis is that water vapour has been transformed into liquid water through the condensation processes that occur within the convection, meaning that water vapour has given way to cloud formation. Of course, this needs further detail studies with more measurements in order to confirm the hypothesis.

Finally, we have also noted contrasted behaviour of the water vapour field with respect to large scale precipitation systems. When this is a large and established synoptic scale frontal passage, the water vapour field appears in phase with the frontal system: the maximum water vapour lies under the front where the air is saturated by rain. However, in the case of low intensity

precipitation front, water vapour depletion appeared in those spots where the convective cells developed, imbedded in the larger system. That seems to indicate that the cell actually feed on the underlying water vapour. That assumption is further confirmed by the fact that the convective front “trails” the water vapour field and develops preferably in those areas where the water vapour densities are the highest.

At this stage, the work performed here has been essentially qualitative but we feel that it has proven useful in pointing out to very interesting mechanisms that link water vapour field distribution and evolution with respect to the precipitating system dynamics and behaviour. Nonetheless, these hypotheses need to be further addressed to draw on definite conclusions. That is the object of currently ongoing studies.

Another aspect of this work has also been to test GPS tomography for water vapour field retrieval using only the GPS and surface data. The restitutions obtained are quite reasonable and allows meaningful interpretations, in particular in the part of the domain where the GPS station density is the highest where we could retrieve higher resolution of the water vapour density field. However, by using only GPS data, the vertical structure of the water vapour field is somewhat reduced unless GPS stations are close enough to form a dense network where multiple rays can cross in individual voxels. Hence, now that we are confident in the GPS tomography method to retrieve 3-D water vapour fields, we plan to improve the current analysis scheme by enhancing the algorithm such that measured profiles of water vapour density within the COPS domain can be accounted for during the inversion initialisation step. That should prove useful in order to render more vertical structures in the tomographic results and avoid the vertical dilution of the GPS signal.

Furthermore, we plan to reprocess the periods of interest with higher resolution both in space (especially in the vertical for levels where multiple rays can cross within individual voxels) and time (down to 20 minutes) in order to refine our comparisons with the radar observations in the core of the COPS domain where the GPS station network is sufficiently dense. This will allow us to further study some these events where we can relate the convective initiation to fine orographic features such as hills within the exit of mountain valleys.

Finally, we will also increase the scope of the present analyses by using other means of observations and supporting atmospheric variables, such as the low level wind from dual Doppler radar analysis as well as VERA analysis, ground based and airborne lidar measurements, etc.. Likewise, we will compare our measurements and field retrievals with model outputs as a way to both validate the corresponding results and to investigate in detail the processes and controlling factors of the precipitation systems lifecycle.

Acknowledgements

The lead author would like to thank the anonymous reviewers for their precise and constructive comments and, in particular, for a series of thought provoking questions and suggestions which, without a doubt, have significantly contributed to the improvement of the article while they have also initiated further investigations in progress.

The COPS campaign implementation and the instrument participation (radars and GPS in this instance) were made possible through the financial support of the DFG Priority Programme 1167

in Germany, and ANR (grant ANR-06-BLAN-0018-04: COPS/France) and CNRS/INSU (LEFE/IDAO program) in France.

REFERENCES

Barthlott C, Richard E, Burton R, Gadian A, Blyth AM, Mobbs S, Bauer H-S, Schwitalla T, Keil C, Trentmann J, Kern B, Seity Y, Kirshbaum D, Hanley K, Handwerker J. 2011. Initiation of deep convection at marginal instability in an ensemble of mesoscale models: A case study from COPS. *Quart. J. Roy. Meteor. Soc.*, this special issue.

Behrendt A, et al. 2011. The impact of the spatiotemporal variability of water vapour on convection initiation in low mountains: Multi-sensor observations during COPS IOP8b; *Quart. J. Roy. Meteor. Soc.*, this special issue.

Bender, M., Dick, G., Wickert, J., Schmidt, T., Song, S., Gendt, G., Ge, M., and Rothacher, M., 2008: Validation of GPS slant delays using water vapour radiometers and weather models. *Meteorologische Zeitschrift*, **17**(6), 807-812.

Bennett, L. J., A.M. Blyth, R.M. Burton, A. Gadian, T.M. Weckwerth, A. Behrendt, P. Di Girolamo, M. Dorninger, S.-J. Lock, V.H. Smith, and S.D. Mobbs, 2011: Initiation of convection over the Black Forest mountains during COPS IOP15a, *Quart. J. Roy. Meteor. Soc.*, this special issue.

Bevis M., S. Businger, T. A. Herring, C. Rocken, R. A. Anthes, and R. H. Ware, 1992: GPS Meteorology: Remote sensing of atmospheric water vapour using the Global Positioning System; *Journal Geophys. Res., 103*, 15787-15801.

Bevis M., S. Businger, S. Chiswell, T. A. Herring, R. A. Anthes, C. Rocken, and R. H. Ware, 1994: GPS Meteorology: Mapping zenith wet delay onto precipitable water; *Journal of Applied Meteorology*, *33*, 379-386.

Boehm, J., Niell, A., Tregoning, P., and Schuh, H., 2006: Global Mapping Function (GMF): A new empirical mapping function based on numerical weather model data. *Geophysical Research Letters*, 33:L07304.

Braun, J., C. Rocken and J. Liljegren, 2003: Comparisons of Line-of-Sight Water Vapour Observations Using the Global Positioning System and a Pointing Microwave Radiometer, *J. of Atmosph. Ocean Techn*.,**20**, 606-612.

Businger S., S.R. Chiswell, M. Bevis, J. Duan, R.A. Anthes, C. Rocken, R.H. Ware, M. Exner, T. VanHove, and F. Solheim, 1996: The promise of GPS in atmospheric monitoring; *Bull. Amer. Meteor. Soc.*, **77**, 5-18.

Champollion, C., C. Flamant, O. Bock, F. Masson, D.D. Turner, T. Weckwerth, 2009: Mesoscale GPS tomography applied to the 12 June 2002 convective initiation event of IHOP_2002; *Quarterly Journal of the Royal Meteorological Society*, **135**, p 645–662; DOI: 10.1002/qj.386.

Champolion, C., F. Masson, M-N Bouin, A. Walpersdorf, E. Doerflinger, O. Bock, J. Van Baelen, 2005 : GPS water vapour tomography : First results from the ESCOMPTE field experiment, *Atmospheric Research*, **74**, 253-274.

Collier, C., F. Davies, J. Davis, G. Pearson, and M. Hagen, 2008: Doppler radar and lidar observations of a thunderstorm outflow, *Proceedings of the fifth European Conference on radar in Meteorology and Hydrology*, Helsinki, Finland, 30 June - 4 July 2008.

Duan J. M. Bevis, P. Fang, Y. Bock, S. Chiswell, S. businger, C. Rocken , F. Solheim, T. VanHove, R. Ware, S. McClusky, T.A. Herring, and R.W. King, 1996: GPS meteorology: direct estimation of the absolute value of precipitable water; *J. Appl. Meteor.*, **35**, 830-838.

Emardson, T. R., and H. J. P. Derks, 1999: On the relation between the wet delay and the integrated precipitable water vapour in the European atmosphere; *Meteorological Applications,* **6**, 1-12.

Flores, A., A. Rius, and G. Ruffini, 2000: 4D tropospheric tomography using GPS slant wet delays, *Ann. Geophys.*, **18**, 223-224.

Flores A., J. Vilà-Guerau de Arellano, L. Gradinarsky, and A. Rius, 2001: Tomography of the Lower Troposphere Using a Small Dense Network of GPS Receivers, *IEEE Transactions on Geoscience and Remote Sensing,* **39 (**2), 439-447.

Gendt, G., Dick, G., Reigber, C., Tomassini, M., Liu, Y., and Ramatschi, M., 2004: Near real time GPS water vapour monitoring for numerical weather prediction in Germany. *Journal of the Meteorological Society of Japan,* **82**(1B):361–370.

Gendt, G., Dick, G., Rius, A., and Sedo, P., 2001: Comparison of software and techniques for water vapour estimation using german near real-time GPS data. *Physics and Chemistry of the Earth* (A), **26**(6-8):417–420.

Gradinarsky L.P., and Jarlemark P., 2004: Ground based GPS tomography of water vapour: analysis of simulated and real data; Journal *of the Meteorological society of Japan,* **82***(1B),* 551-560.

Ha, S-Y., Y.-H Kuo and Y.-R, Guo, 2003: Variational Assimilation of Slant-Path Wet Delay Measurements from a Hypothetical Ground-Based GPS Network. Part I: Comparison with Precipitable Water Assimilation, *Mon. Wea. Rev.*,**131**, 2635-2655.

Hagen, M., J. van Baelen, E. Richard, 2011 : Influence of the Wind Profile on the Initiation of Convection in Mountainous Terrain ; *Quart. J. Roy. Meteor. Soc.*, this special issue.

Kottmeier, Ch., N. Kalthoff, Ch. Barthlott, U. Corsmeier, J. Van Baelen, A. Behrendt, R. Behrendt, A. Blyth, R. Coulter, S. Crewell, P. Di Giromalo, M. Dorninger, C. Flamant, Th. Foken, M. Hagen, C. Hauck, H. Höller, H. Konow, M. Kunz, H. Mahlke, S. Mobbs, E. Richard, R. Steinacker, T. Weckwerth, A. Wieser, and V. Wulfmeyer, 2008: Mechanisms initiating deep convection over complex terrain during COPS. *Meteorol. Z.*, **17**, 931-948.

Liljegren J.C., B.M. Lesht, T. VanHove, and C. Rocken,1999, "A comparison of integrated water vapor from microwave radiometer, balloon-borne sounding system, and global positionnng system", *Ninth ARM Science Team Meeting*, San Antonio, TX, March 22-26, 1999.

Liu, H., and M. Xue, 2006: Retrieval of Moisture from Slant-Path Water Vapour Observations of a Hypothetical GPS Network Using a Three-Dimensional Variational Scheme with Anisotropic Background Error, *Mon. Wea. Rev.*, **134**, 933-949.

MacDonald, A., Y. Xie and R. Ware, 2002: Diagnosis of Three Dimensional Water Vapour Using Slant Observations from a GPS Network, *Mon. Wea. Rev.*, **130**, 386-397.

McClatchey, R. A., R. W. Fenn, J.E.A. Selby, F. E. Volz, and J. S. Garing, 1972: Optical properties of the atmosphere, AFCRL-72-0497, 108 pp.

Menke W., 1989: Geophysical Data Analysis: Discrete Inverse Theory; *Academic Press*, London, United Kingdom.

Niell, A. E., 1996: Global mapping functions for the atmosphere delay at radio wavelengths, *Journal of Geophysical Research*, **101**(B2):3227–3246.

Planche C, Wobrock W, Flossmann AI, Tridon F, Van Baelen J, Pointin Y, Hagen M., 2010 : The influence of aerosol particle number and hygroscopicity on the evolution of convective cloud systems and their precipitation: A numerical study based on the COPS observations on 12 August 2007. *Atmos. Res*. In press. DOI: 10.1016/j.atmosres.2010.05.003.

Reverdy, M., 2008: Estimation des paramètres atmosphériques par GPS: analyse de la variabilité spatio-temporelle de la vapeur d'eau, Thesis of the Université Blaise Pascal, Clermont-Ferrand, France, n°598, 264pp.

Reverdy, M, Van Baelen J, Walpersdorf A, Dick G, Hagen M, Richard E. 2009: Water vapour fields retrieval with tomography software. *Ann. Meteorol*. **44**: Deutscher Wetterdienst, Offenbach. ISBN 978-3-88148-440-4, 144-145. www.pa.op.dlr.de/icam2009/extabs

Richard, E., C. Flamant, F. Bouttier, J. Van Baelen, C. Champollion, M. Hagen, J. Cuesta, P. Bosser, G. Pigeon, S. Argence, J. Arnault, P. Brousseau, Y. Seity, J.-P. Chaboureau, P.

Limnaios, F. Masson, Y. Pointin, P. Di Girolamo, V. Wulfmeyer, 2009 : La campagne COPS : Initiation et cycle de vie de la convection en région montagneuse, *La Météorologie*, **64**, 32-42.

Richard E, Chaboureau J-P, Flamant C, Champollion C, Hagen M, Schmidt K, Kiemle C, Corsmeier C, Barthlott C., 2011: Forecasting Summer convection over the Black Forest: a case study from the COPS experiment. *Quart. J. Roy. Meteor. Soc.*, this special issue.

Schroth, A.C., M.S. Chandra, and P.F. Mesichner, 1988: A *C*-Band Coherent Polarimetric Radar for Propagation and Cloud Physics Research. *J. Atmos. Ocean. Technol.*, **5**, 803–822.

Saastamoinen, J., 1972: Atmospheric correction for the troposphere and stratosphere in radio ranging of satellites; *The use of Artificial Satellites for Geodesy*, **15**, *Geophysical Monograph*, 247-251, Amer.. Geophys. Union, Washington D.C., USA.

Solheim, F., J. Vivekanandan, R. Ware and C. Rocken, 1999: Propagation Delays Induced in GPS Signals by Dry Air, Water Vapour, Hydrometeors and other Atmospheric Particulates, *J. Geophys Res.*, **104** (D8), 9663-9670.

Steinacker, R., M. Ratheiser, B. Bica, B. Chimani, M. Dorninger, W. Gepp, C. Lotteraner, S. Schneider, and S. Tschannett, 2006: A Mesoscale Data Analysis and Downscaling Method over Complex Terrain. *Mon. Wea. Rev.*, **134**, 2758–2771.

Tarantola A., 2005: Inverse Problem Theory and methods for model parameter estimation, *Society for industrial and applied mathematics*, Philadelphia, USA.

Tregoning P., R. Boers, D. O'Brien, and M. Hendy, 1998: Accuracy of absolute precipitable water vapour estimates from GPS observations; *J. Geophys. Res*., **103**, 28701-28710.

Van Baelen, J., J-P Aubagnac, A. Dabas, 2005 : Comparison of near real-time estimates of integrated water vapour derived with GPS, radiosondes, and microwave radiometer, *J. of Atmosph. Ocean Techn*., **22**, 201-210.

Van Baelen, J., and G. Penide, 2009 : Study of water vapour vertical variability and possible cloud formation with a small network of GPS stations, *Geophys. Res. Lett*., **36**, L02804, doi:10.1029/2008GL036148.

Wang J., L. Zhang, A. Dai, T. Van Hove, J. Van Baelen, 2007 : A near-global 2-hourly data set of atmospheric precipitable water from ground-based GPS measurements, J. of Geophys. Res., 2007, 112D11D11107.

Ware, R., C. Alber, C. Rocken and F. Solheim, 1997: Sensing integrated water vapour along GPS ray paths, *Geophys. Res. Let*., **24**, 417-420.

Wulfmeyer, V., A. Behrendt, H.S. Bauer, C. Kottmeier, U. Corsmeier, A. Blyth, G. Craig, U. Schumann, M. Hagen, S. Crewell, P. Di Girolamo, C. Flamant, M. Miller, A. Montani, S. Mobbs, E. Richard, M.W. Rotach, M. Arpagaus, H. Russchenberg, P. Schlüssel, M. König, V. Gärtner, R. Steinacker, M. Dorninger, D.D. Turner, T. Weckwerth, A. Hense, and C. Simmer,

2008: RESEARCH CAMPAIGN: The Convective and Orographically Induced Precipitation Study. *Bull. Amer. Meteor. Soc.*, **89**, 1477–1486.

Wulfmeyer V, Behrendt A, Kottmeier C, Corsmeier U, Barthlott C, Craig G, Hagen M, Althausen D, Aoshima, F, Arpagaus M, Bauer HS, van Baelen J, Bennett, L, Blyth A, Brandau C, Champollion C, Crewell S, Dick G, Dorninger M, Dufournet Y, Eigenmann R, Engelmann R, Flamant C, Foken T, Di Girolamo P, Groenemeijer P, Gorgas T, Grzeschik M, Peters G, Handwerker J, Hauck C, Höller H, Junkermann W, Kalthoff N, Kiemle C, König M, Krauss L, Long C, Madonna F, Mobbs S, Neininger B, Pal S, Pigeon G, Richard E, Rotach MW, Russchenberg H, Schwitalla, T, Smith V, Steinacker R, Trentmann J, Turner DD, Vogt S, Volkert H, Weckwerth T, Wernli H, Wieser, A., 2011: The Convective and Orographically Induced Precipitation Study (COPS): The scientific strategy, the field phase, and first highlights. *Quart. J. Roy. Meteor. Soc.*, this special issue.

Zumberge, J. F., Heflin, M. B., Jefferson, D. C.,Watkins, M. M., andWebb, F. H., 1997: Precise point positioning for the efficient and robust analysis of GPS data from large networks, *Journal of Geophysical Research*, **102**(B3):5005–5018.

Figure Captions:

Figure 1: The COPS campaign domain with the GPS stations network (white dots), the POLDIRAD (P) weather radar location (white diamond) with its 120 km radius field of view circle, and the instrumentation supersites (white squares) with, from West to East, the Vosges low mountain site (V), the Rhine valley site (R), the Hornisgrinde mountain site (H), the Murg valley site (M), and the Deckenpfronn site near Stuttgart (S). The main orographic features are also indicated: the Vosges Mountains to the West, the Rhine Valley in the centre, and the Black Forest Mountains to the East.

Figure 2: POLDIRAD reflectivity PPI observations of the heavy precipitation isolated cell on July 15, 2007 (IOP 8b) at 14:20, 14:40, 15:00, and 15:20 UTC, respectively. The colour scale indicates the reflectivity from -10 to 60 DBz.

Figure 3a : GPS IWV 2-D fields (left column) and tomography horizontal water vapour density fields at the 1000 m height layer (right column) from 13:00 to 15:00 UTC on July 15, 2007 (IOP 8b). The IWV scale goes from 5 to 40 mm and the water vapour density scale goes from 4 to 14 g/m^3. The black circle indicates the area of convective activity seen on the radar display of Figure 2.

Figure 3b: IWV time series for July 15, 2007 (IOP 8b: Day 196) for the four surrounding GPS stations around the area of convective activity at 15:00 UTC in the Black Forest (black circle on the previous figure). Positions on the plots correspond to the relative cardinal positions of the GPS stations.

Figure 4: POLDIRAD reflectivity PPI observations on July 20, 2007 (IOP 9c) at 10:00, and 10:30 UTC, respectively (left column) and GPS IWV field (top right panel) and tomography horizontal water vapour density field for the 1000 m (bottom right panel) height layer at 10:00 UTC on July 20, 2007 (IOP 9c). The radar reflectivity scale goes from -10 to 60 DBz. The IWV scale goes from 17 to 42 mm and the water vapour density scale goes from 6 to 16 g/m^3.

Figure 5: POLDIRAD reflectivity PPI observations on July 18, 2007 (IOP 9a) at 17:00, 17:30, 18:22, and 18:54 UTC, respectively. The colour scale indicates the reflectivity from -10 to 60 DBz.

Figure 6a: GPS tomography horizontal water vapour density fields for the 1000 m height layer from 14:00 to 19:00 UTC, on July 18, 2007 (IOP 9a). The water vapour density scale goes from 4 to 14 g/m^3. The Bruche and Giessen valleys are indicated.

Figure 6b: GPS tomography vertical water vapour density cross-sections at constant latitude 48.64° N (left column) and 48.19° N (right column) from 15:00 to 17:00 and 16:00 to 18:00 UTC, respectively, on July 18, 2007 (IOP 9a). The water vapour density scale goes from 6 to 14 g/m^3.

Figure 7: Supersite Vosges UHF wind profiler time/height plot for July 18, 2007 (IOP 9a). Colour scale indicates wind amplitude in m/s while arrows indicate wind direction.

Figure 8: POLDIRAD reflectivity PPI observations on August 12, 2007 (IOP 15a) at 12:20, 13:20, 14:20 and 15:20 UTC, respectively. The colour scale indicates the reflectivity from -10 to 60 DBz.

Figure 9a : GPS tomography horizontal water vapour density fields for the 1000 m height layer for the 9:00, 11:00, 13:00, and 15:00 UTC time frames, respectively, on August 12, 2007 (IOP 15a). The water vapour density scale goes from 4 to 14 g/m^3. The dash lines indicate the vertical cross-sections of Figure 9b.

Figure 9b : GPS tomography vertical water vapour density cross-sections at constant latitude 48.41° N (left column) and 48.19° N (right column) from 12:00 to 14:00 and 13:00 to 15:00 UTC, respectively, on August 12, 2007 (IOP 15a). The water vapour density scale goes from 5 to 11 g/m^3.

Figure 10 : POLDIRAD reflectivity PPI observations on August 12, 2007 at 21:00, 22:00, 23:00, and August 13, 2007 at 00:00 UTC (IOP 15) respectively (left column) and GPS tomography horizontal water vapour density fields at the 1000 m height layer for the same times (right column). The radar reflectivity scale goes from -10 to 60 DBz. The water vapour density scale goes from 3 to 13 g/m^3.

Figure 11 : POLDIRAD reflectivity PPI observations of isolated cells on August 13, 2007 (IOP 15b) at 13:00, 14:10, 15:21, and 16:30 UTC, respectively. The colour scale indicates the reflectivity from -10 to 60 DBz.

Figure 12a : GPS tomography horizontal water vapour density cuts for the 1000 m height layer from 11:00 to 16:00 UTC, on August 13, 2007 (IOP 15b). The water vapour density scale goes from 3 to 13 g/m^3. The dash lines indicate the vertical cross-sections of Figure 12b and 12c.

Figure 12b : GPS tomography vertical water vapour density cross-sections at constant latitude 48.41° N (left column) and 48.19° N (right column) from 12:00 to 14:00 and 15:00 to 17:00 UTC, respectively, on August 13, 2007 (IOP 15b). The water vapour density scale goes from 5 to 11 g/m^3.

Figure 12c : GPS tomography vertical water vapour density cross-sections at constant longitude 7.34° E from 11:00 to 16:00 UTC, on August 13, 2007 (IOP 15b). The water vapour density scale goes from 5 to 11 g/m^3.

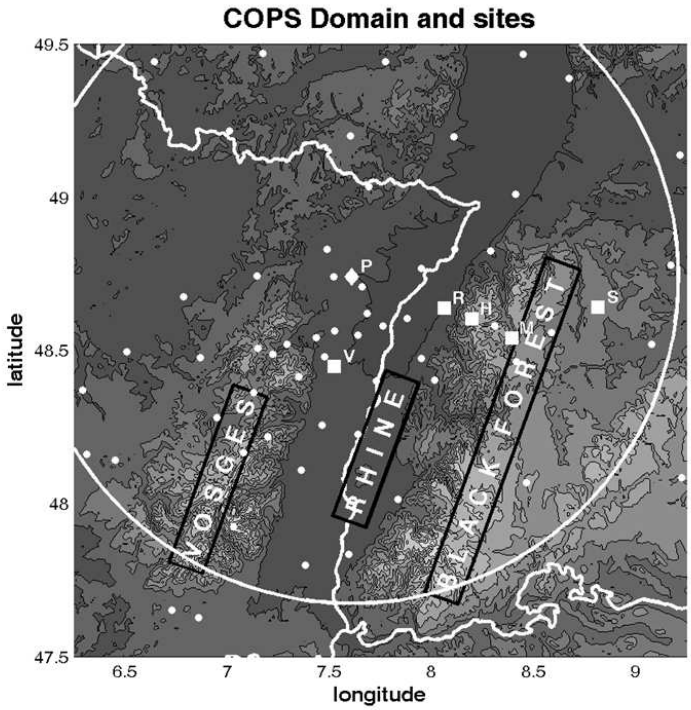

The COPS campaign domain with the GPS stations network (white dots), the POLDIRAD (P) weather radar location (white diamond) with its 120 km radius field of view circle, and the instrumentation supersites (white squares) with, from West to East, the Vosges low mountain site (V), the Rhine valley site (R), the Hornisgrinde mountain site (H), the Murg valley site (M), and the Deckenpfronn site near Stuttgart (S). The main orographic features are also indicated: the Vosges Mountains to the West, the Rhine Valley in the centre, and the Black Forest Mountains to the East.

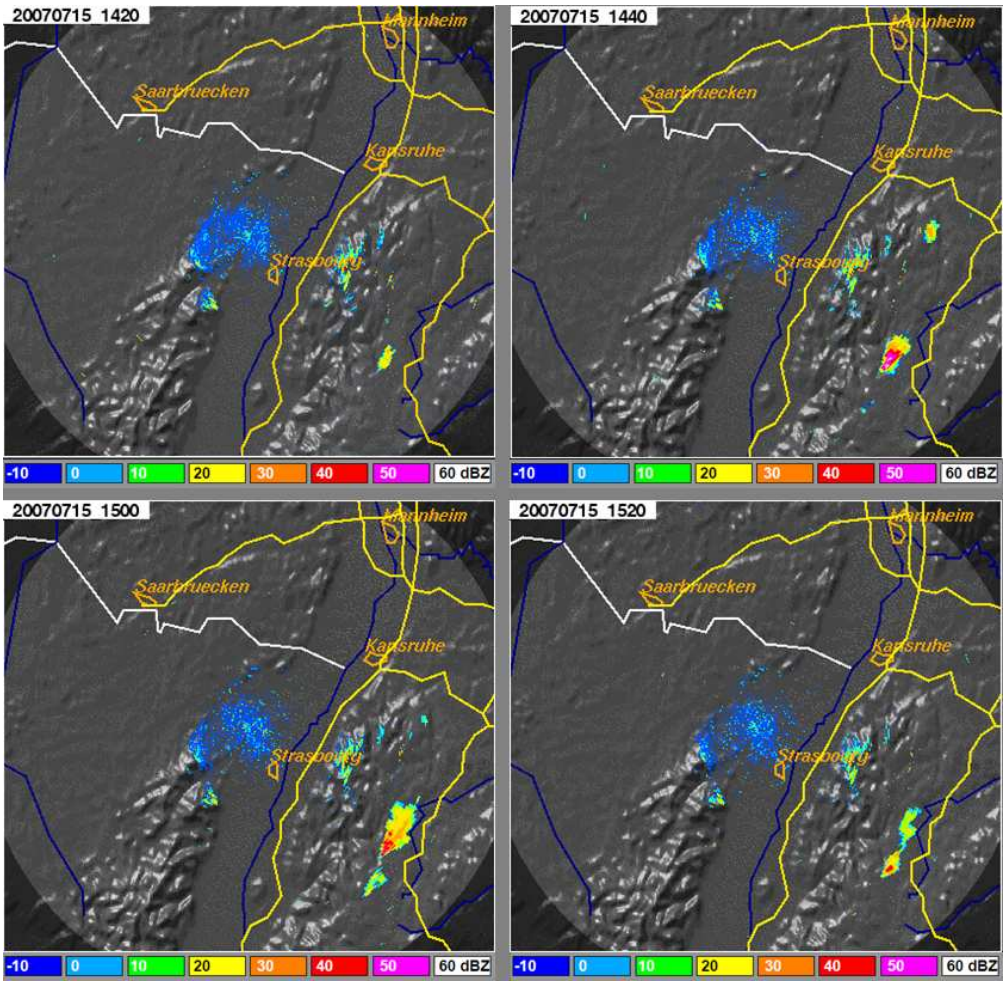

POLDIRAD reflectivity PPI observations of the heavy precipitation isolated cell on July 15, 2007 (IOP 8b) at 14:20, 14:40, 15:00, and 15:20 UTC, respectively. The colour scale indicates the reflectivity from -10 to 60 DBz.

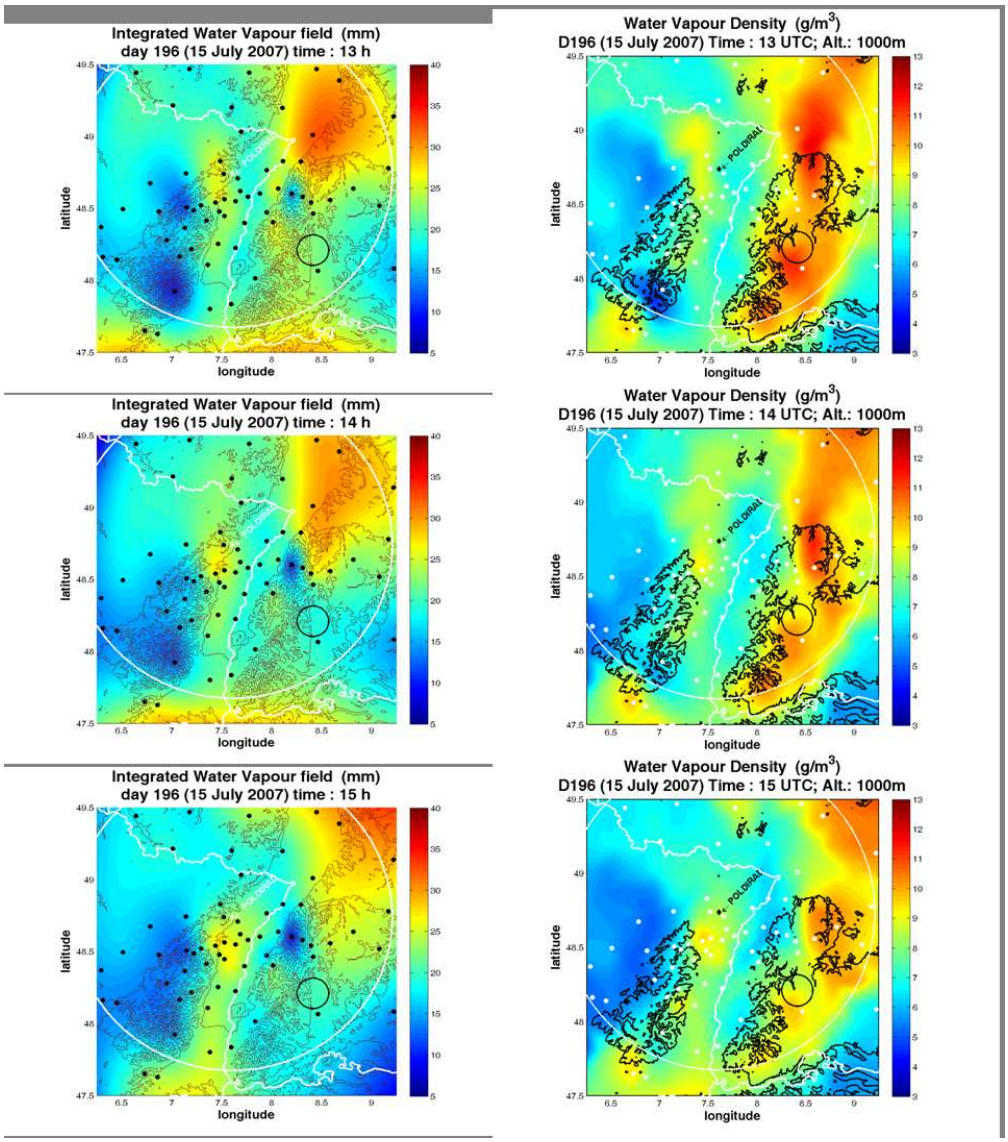

GPS IWV 2-D fields (left column) and tomography horizontal water vapour density fields at the 1000 m height layer (right column) from 13:00 to 15:00 UTC on July 15, 2007 (IOP 8b). The IWV scale goes from 5 to 40 mm and the water vapour density scale goes from 4 to 14 g/m3. The black circle indicates the area of convective activity seen on the radar display of Figure 2.

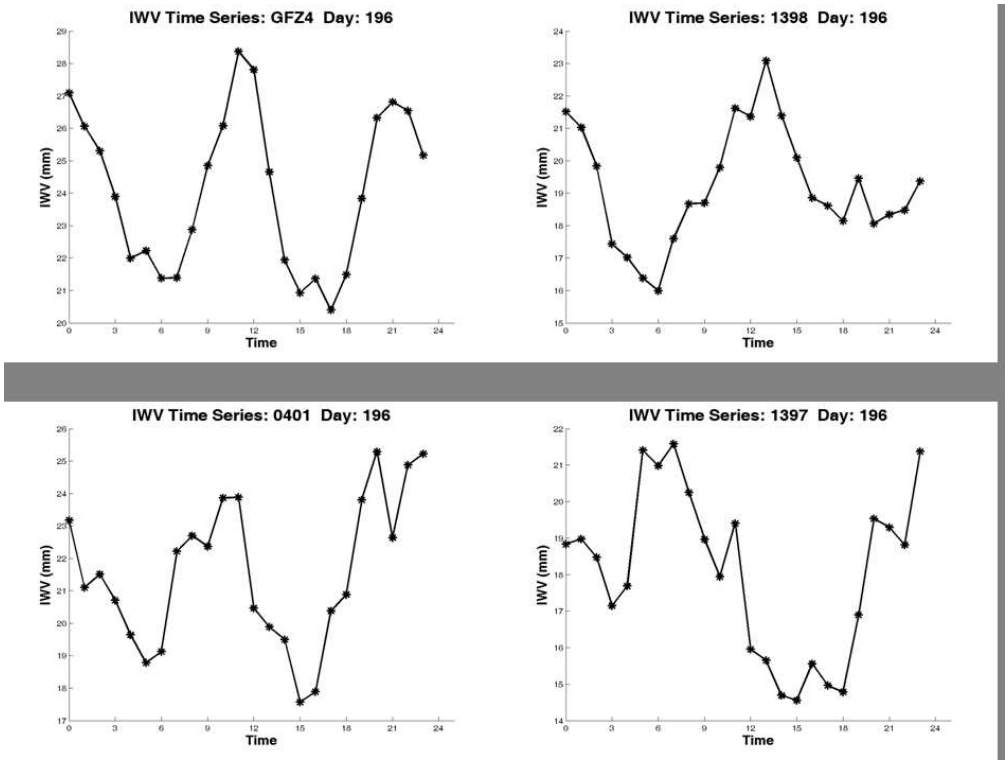

IWV time series for July 15, 2007 (IOP 8b: Day 196) for the four surrounding GPS stations around the area of convective activity at 15:00 UTC in the Black Forest (black circle on the previous figure). Positions on the plots correspond to the relative cardinal positions of the GPS stations.

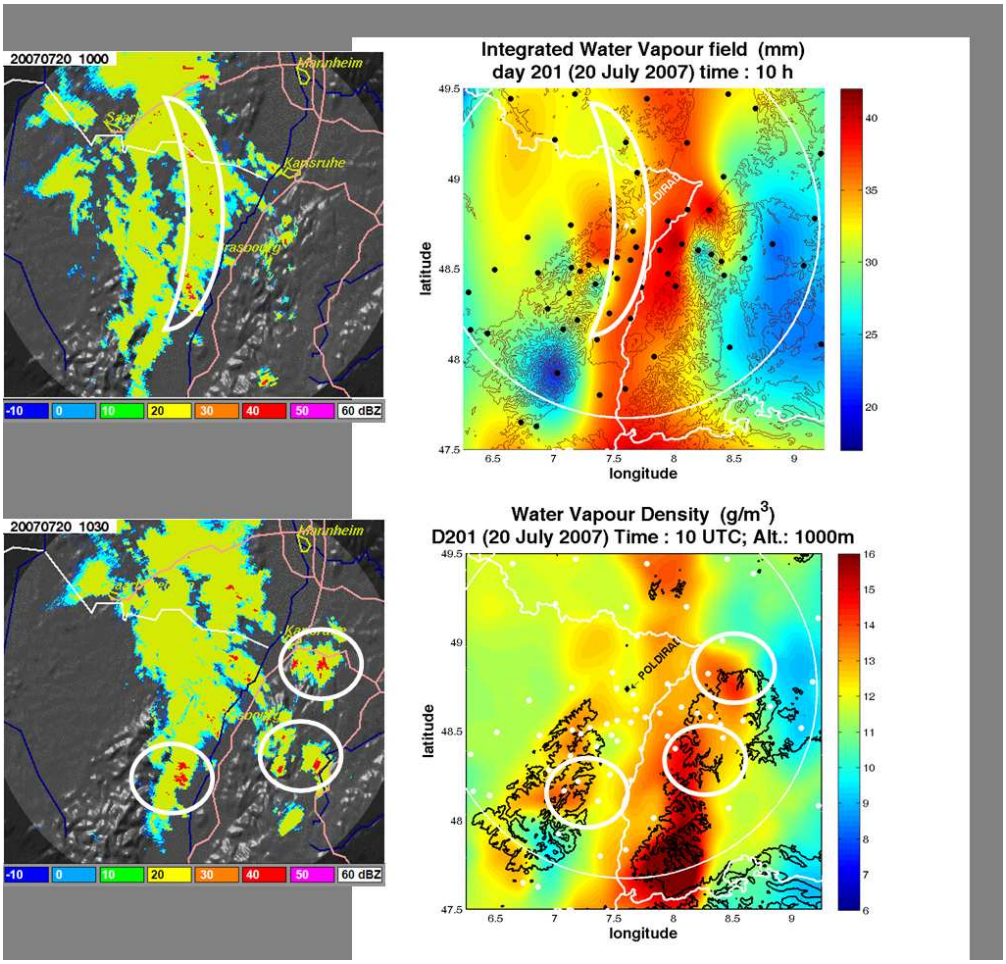

POLDIRAD reflectivity PPI observations on July 20, 2007 (IOP 9c) at 10:00, and 10:30 UTC, respectively (left column) and GPS IWV field (top right panel) and tomography horizontal water vapour density field for the 1000 m (bottom right panel) height layer at 10:00 UTC on July 20, 2007 (IOP 9c). The radar reflectivity scale goes from -10 to 60 DBz. The IWV scale goes from 17 to 42 mm and the water vapour density scale goes from 6 to 16 g/m3.

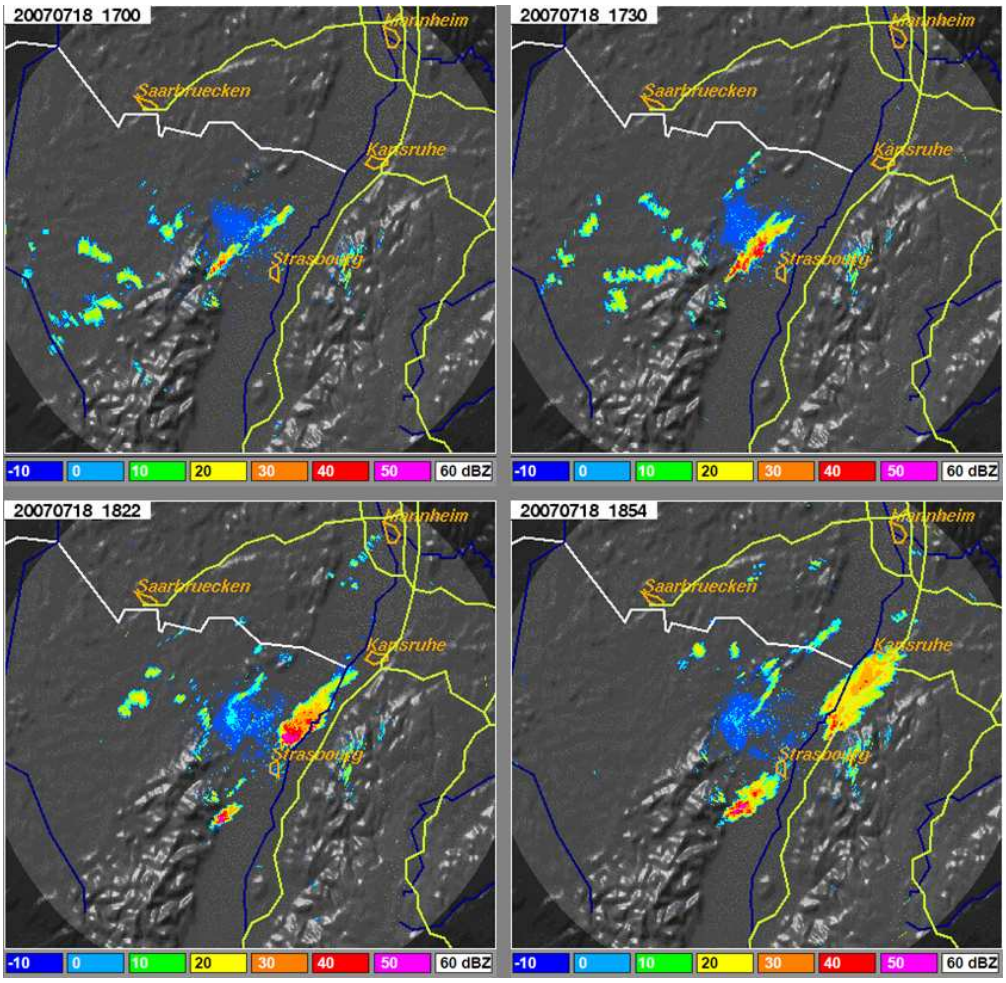

POLDIRAD reflectivity PPI observations on July 18, 2007 (IOP 9a) at 17:00, 17:30, 18:22, and 18:54 UTC, respectively. The colour scale indicates the reflectivity from -10 to 60 DBz.

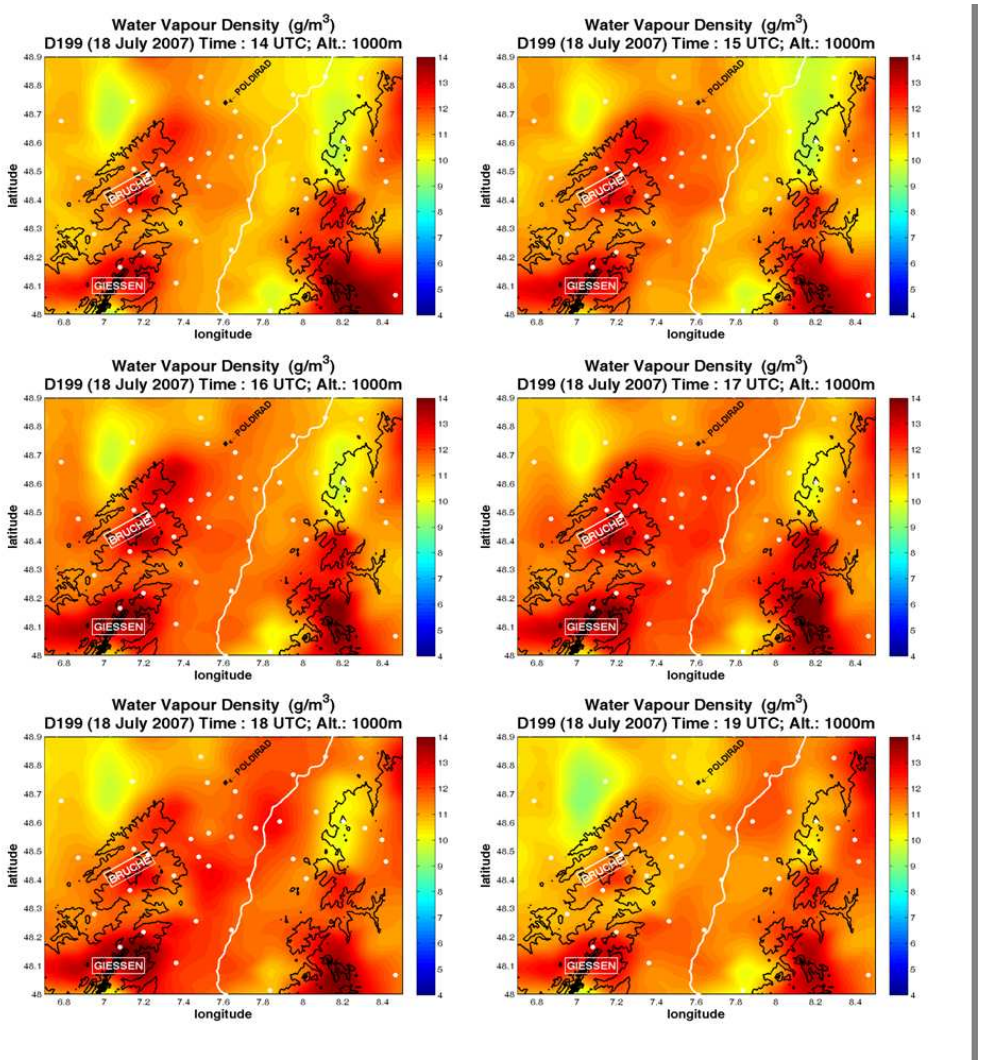

GPS tomography horizontal water vapour density fields for the 1000 m height layer from 14:00 to 19:00 UTC, on July 18, 2007 (IOP 9a). The water vapour density scale goes from 4 to 14 g/m3. The Bruche and Giessen valleys are indicated.

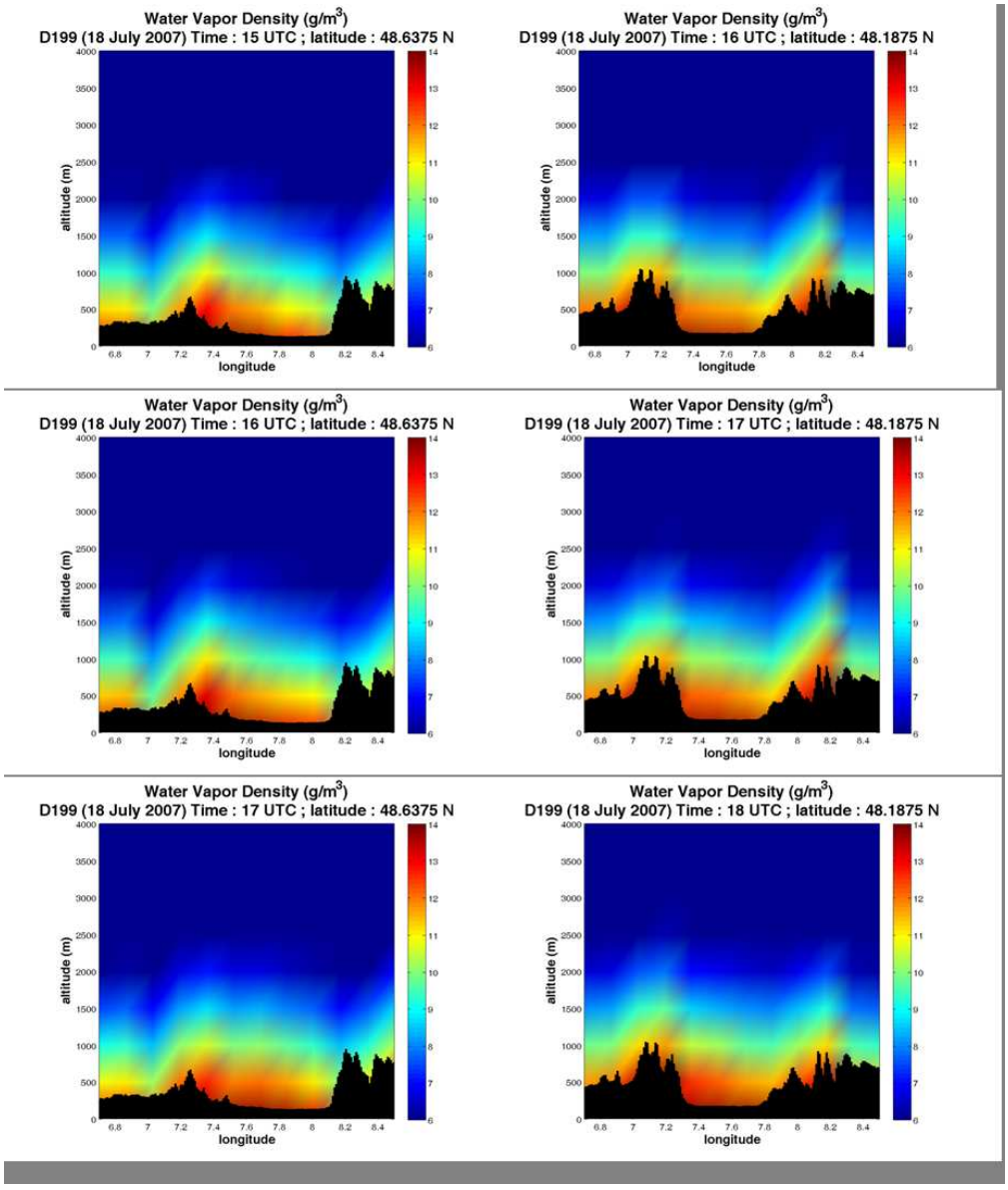

GPS tomography vertical water vapour density cross-sections at constant latitude 48.64° N (left column) and 48.19° N (right column) from 15:00 to 17:00 and 16:00 to 18:00 UTC, respectively, on July 18, 2007 (IOP 9a). The water vapour density scale goes from 6 to 14 g/m3.

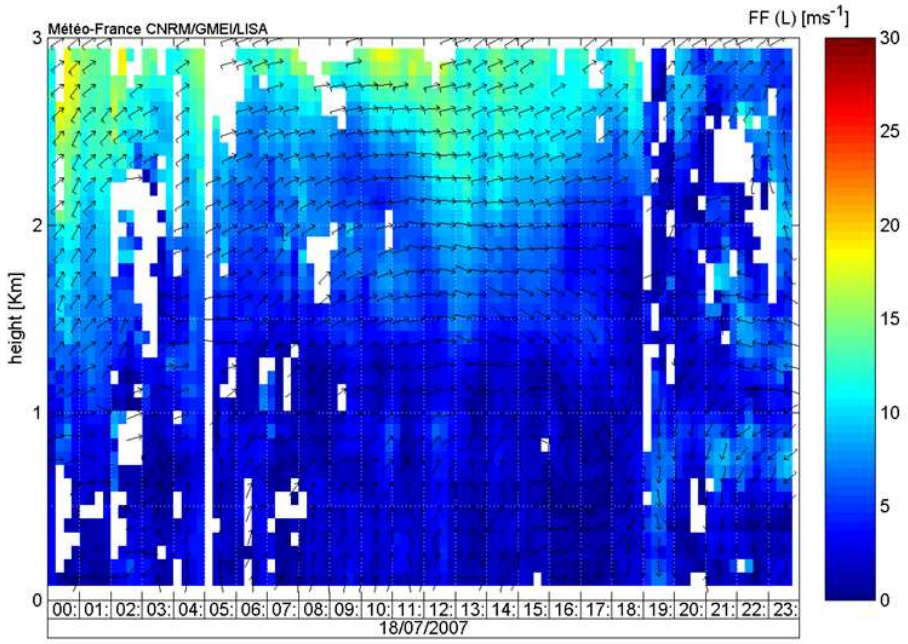

Supersite Vosges UHF wind profiler time/height plot for July 18, 2007 (IOP 9a). Colour scale indicates wind amplitude in m/s while arrows indicate wind direction.

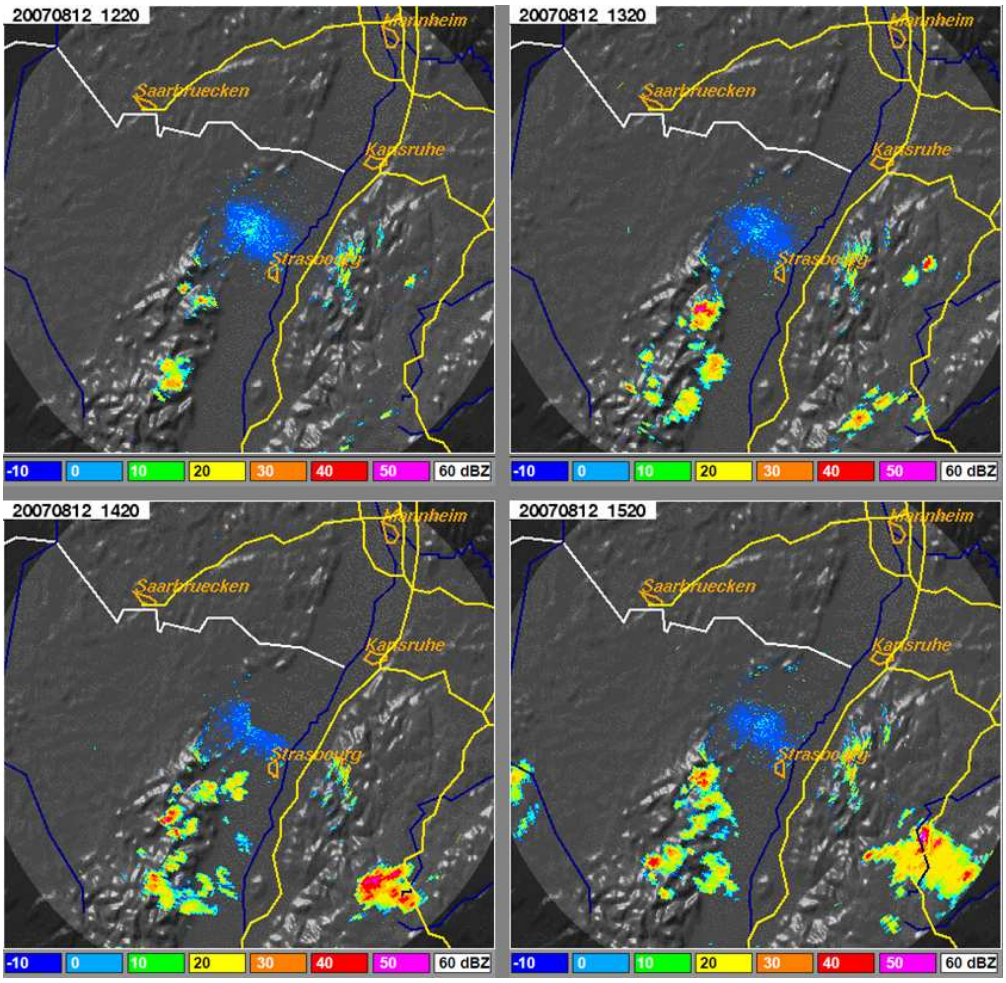

POLDIRAD reflectivity PPI observations on August 12, 2007 (IOP 15a) at 12:20, 13:20, 14:20 and 15:20 UTC, respectively. The colour scale indicates the reflectivity from 10 to 60 DBz.

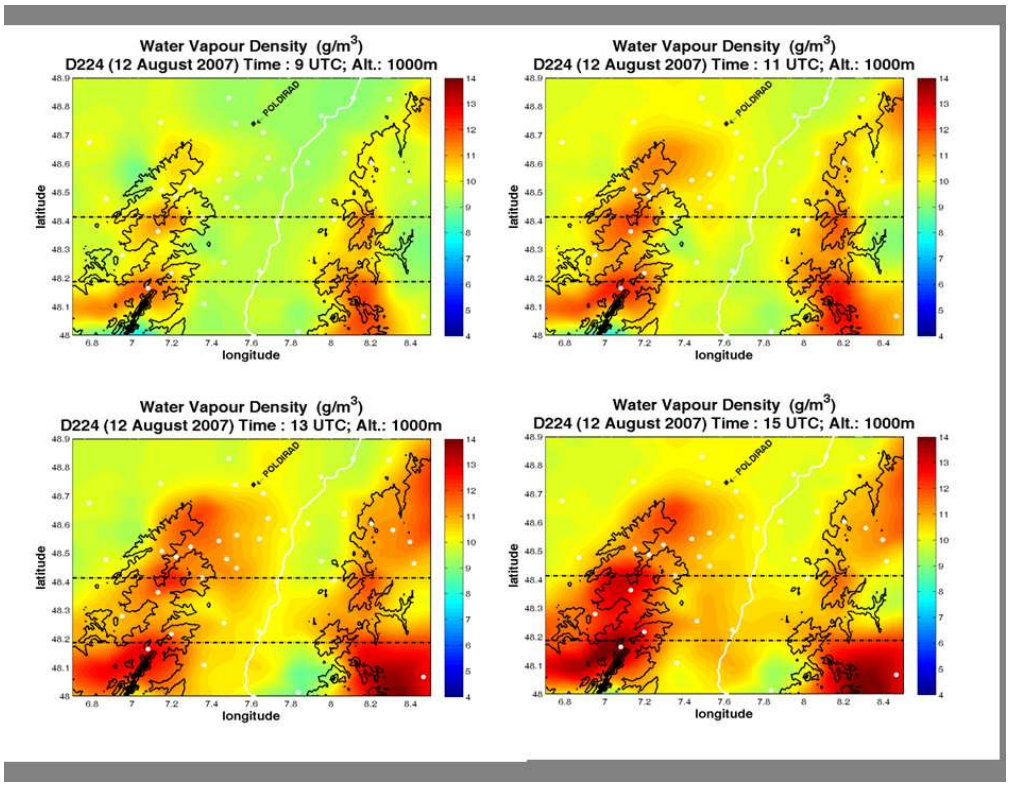

GPS tomography horizontal water vapour density fields for the 1000 m height layer for the 9:00, 11:00, 13:00, and 15:00 UTC time frames, respectively, on August 12, 2007 (IOP 15a). The water vapour density scale goes from 4 to 14 g/m3. The dash lines indicate the vertical cross-sections of Figure 9b.

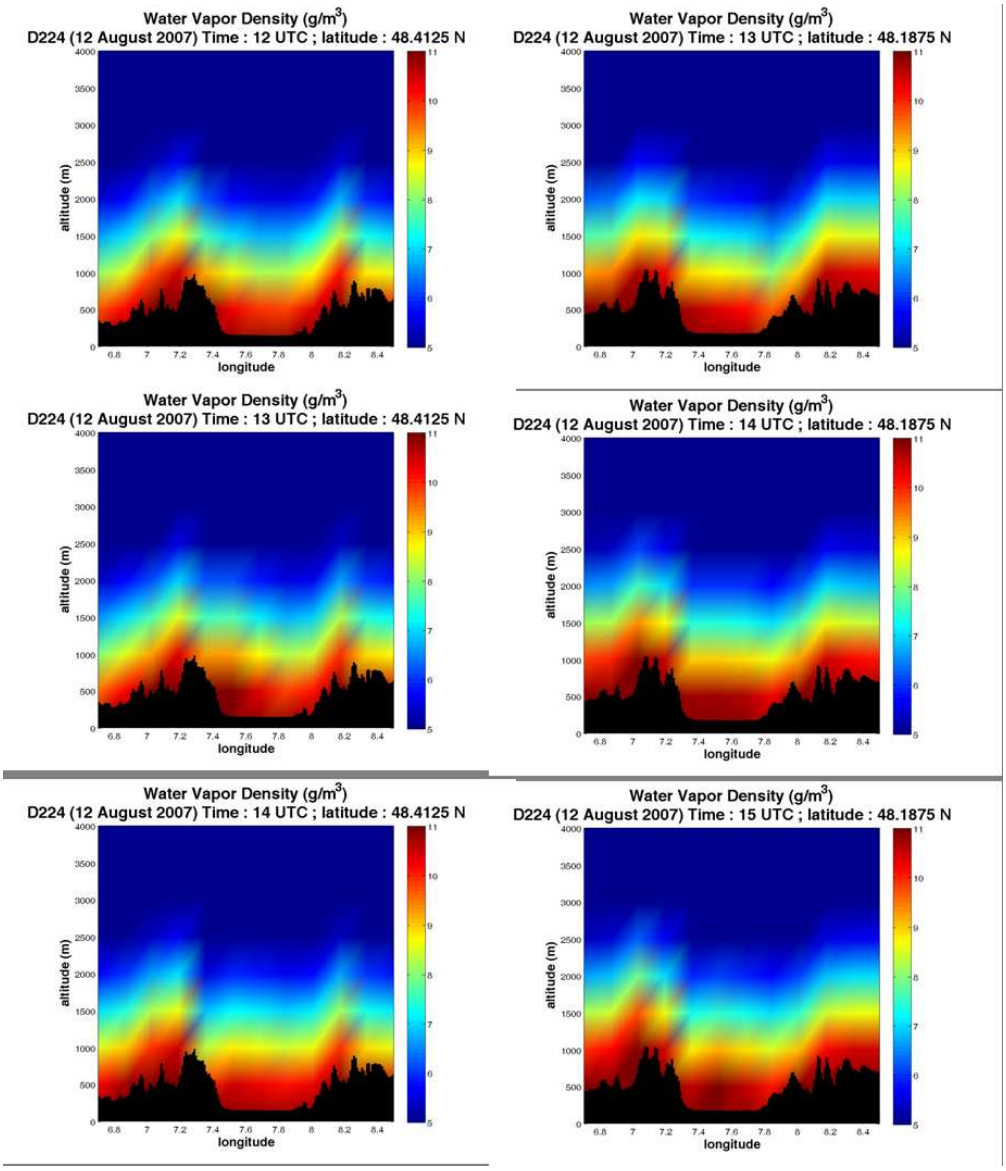

GPS tomography vertical water vapour density cross-sections at constant latitude 48.41° N (left column) and 48.19° N (right column) from 12:00 to 14:00 and 13:00 to 15:00 UTC, respectively, on August 12, 2007 (IOP 15a). The water vapour density scale goes from 5 to 11 g/m3.

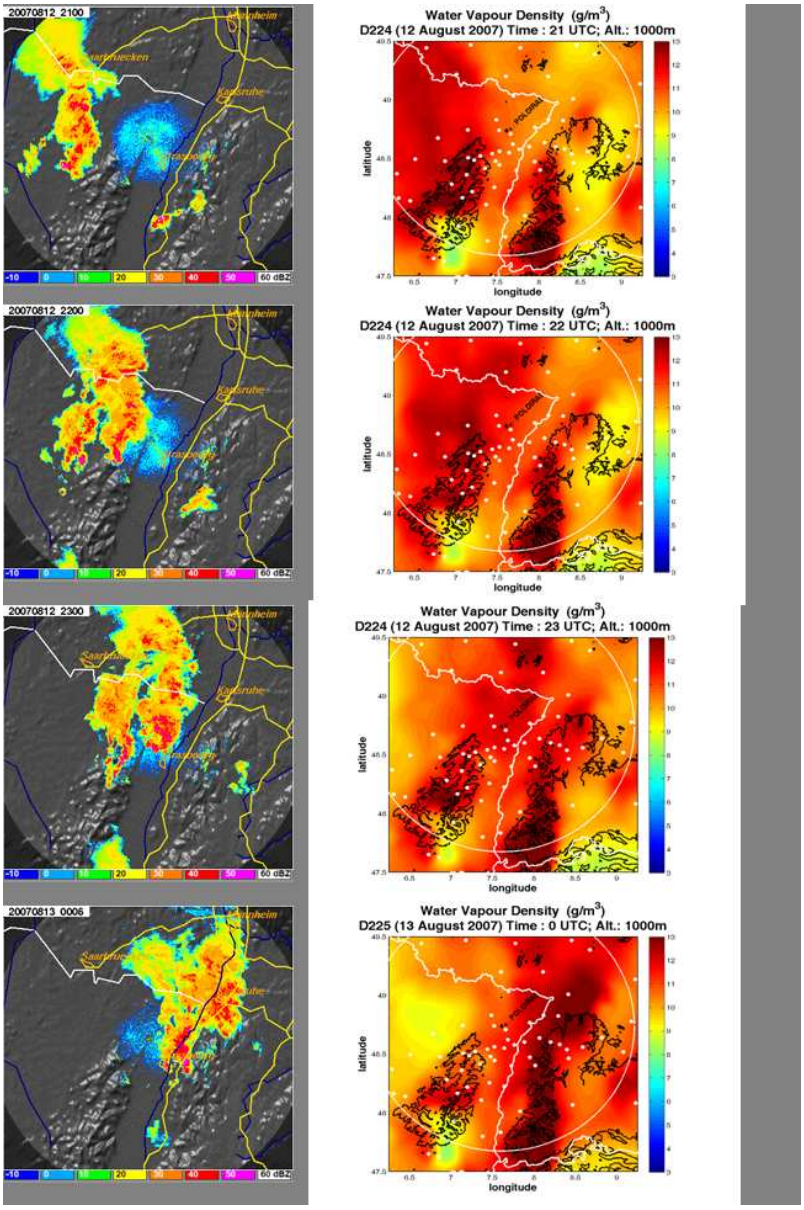

POLDIRAD reflectivity PPI observations on August 12, 2007 at 21:00, 22:00, 23:00, and August 13, 2007 at 00:00 UTC (IOP 15) respectively (left column) and GPS tomography horizontal water vapour density fields at the 1000 m height layer for the same times (right column). The radar reflectivity scale goes from -10 to 60 DBz. The water vapour density scale goes from 3 to 13 g/m3.

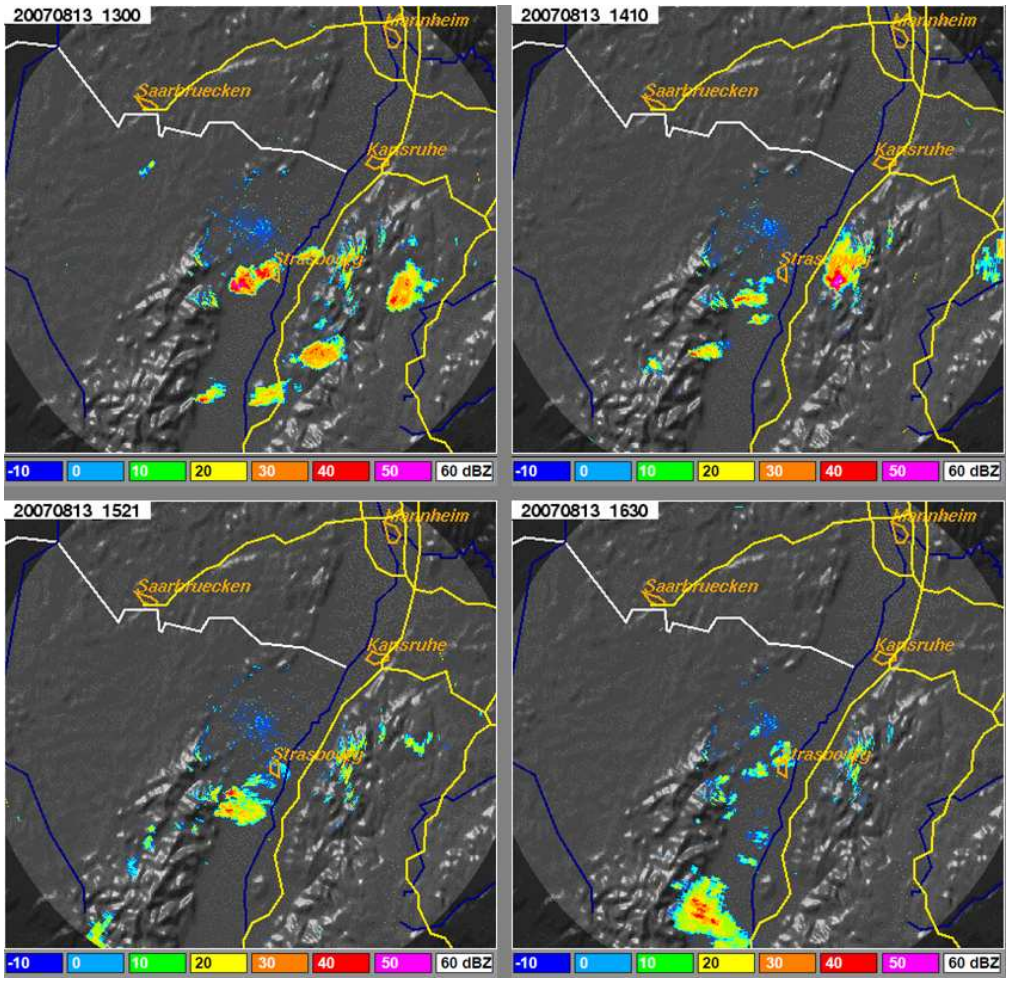

POLDIRAD reflectivity PPI observations of isolated cells on August 13, 2007 (IOP 15b) at 13:00, 14:10, 15:21, and 16:30 UTC, respectively. The colour scale indicates the reflectivity from -10 to 60 DBz.

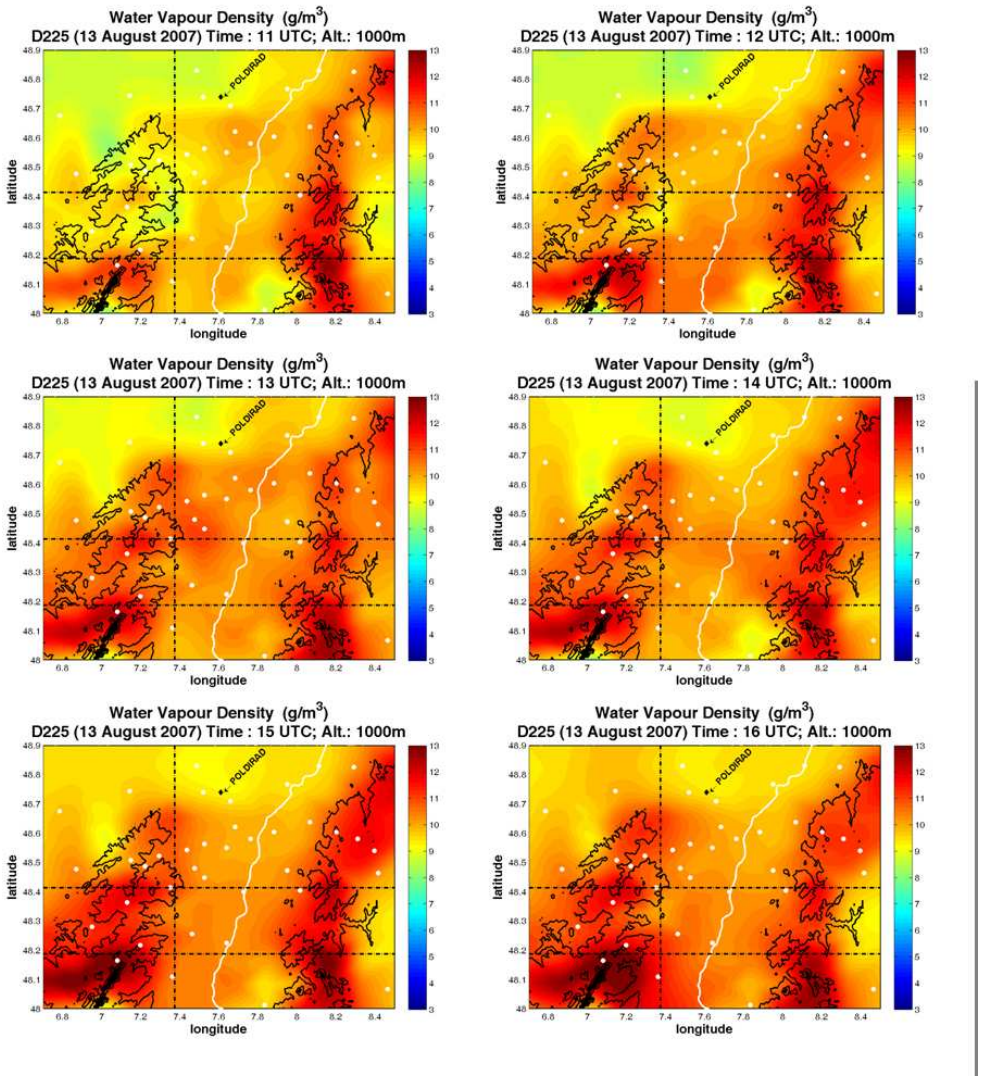

GPS tomography horizontal water vapour density cuts for the 1000 m height layer from 11:00 to 16:00 UTC, on August 13, 2007 (IOP 15b). The water vapour density scale goes from 3 to 13 g/m3. The dash lines indicate the vertical cross-sections of Figure 12b and 12c.

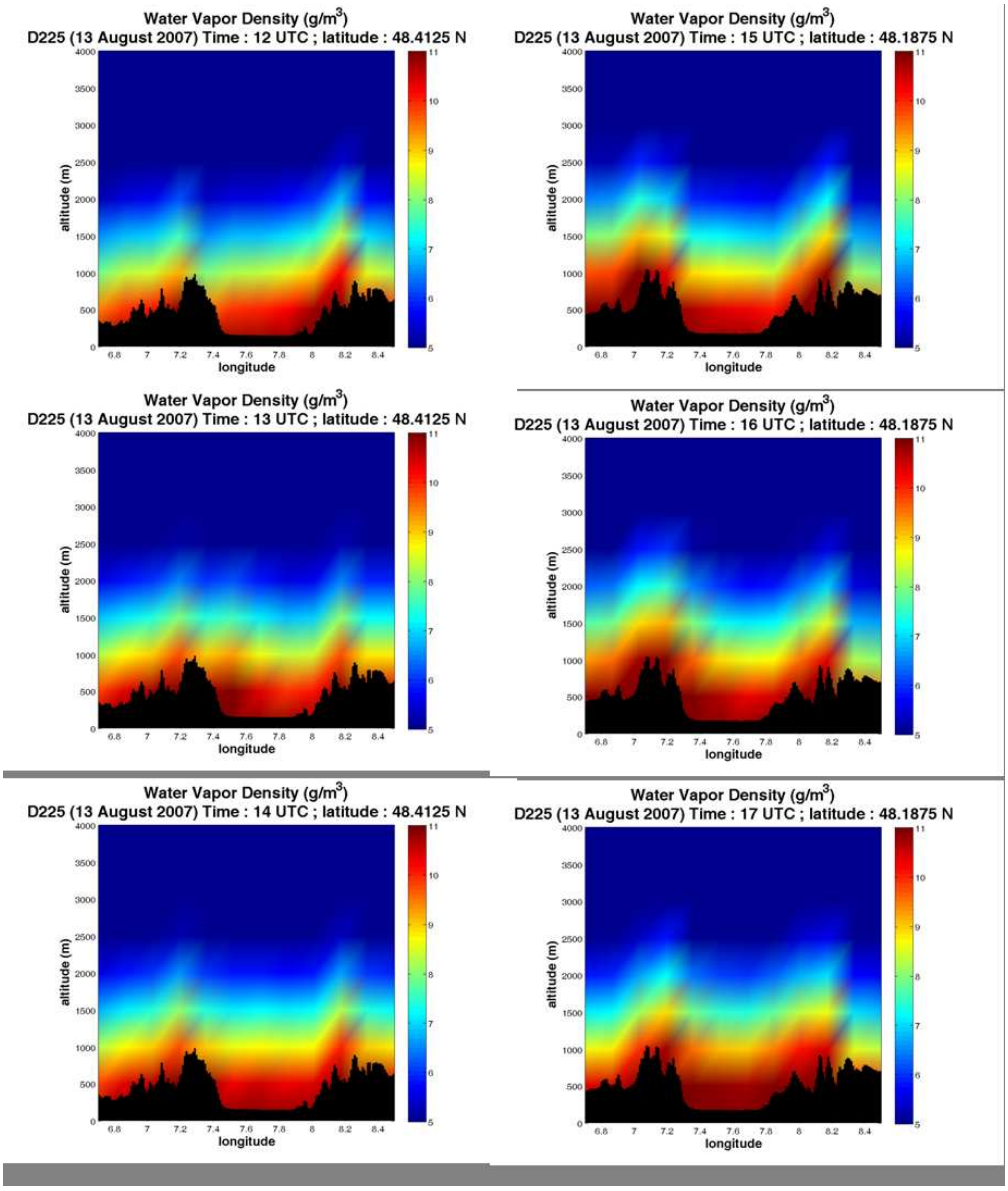

GPS tomography vertical water vapour density cross-sections at constant latitude 48.41° N (left column) and 48.19° N (right column) from 12:00 to 14:00 and 15:00 to 17:00 UTC, respectively, on August 13, 2007 (IOP 15b). The water vapour density scale goes from 5 to 11 g/m3.

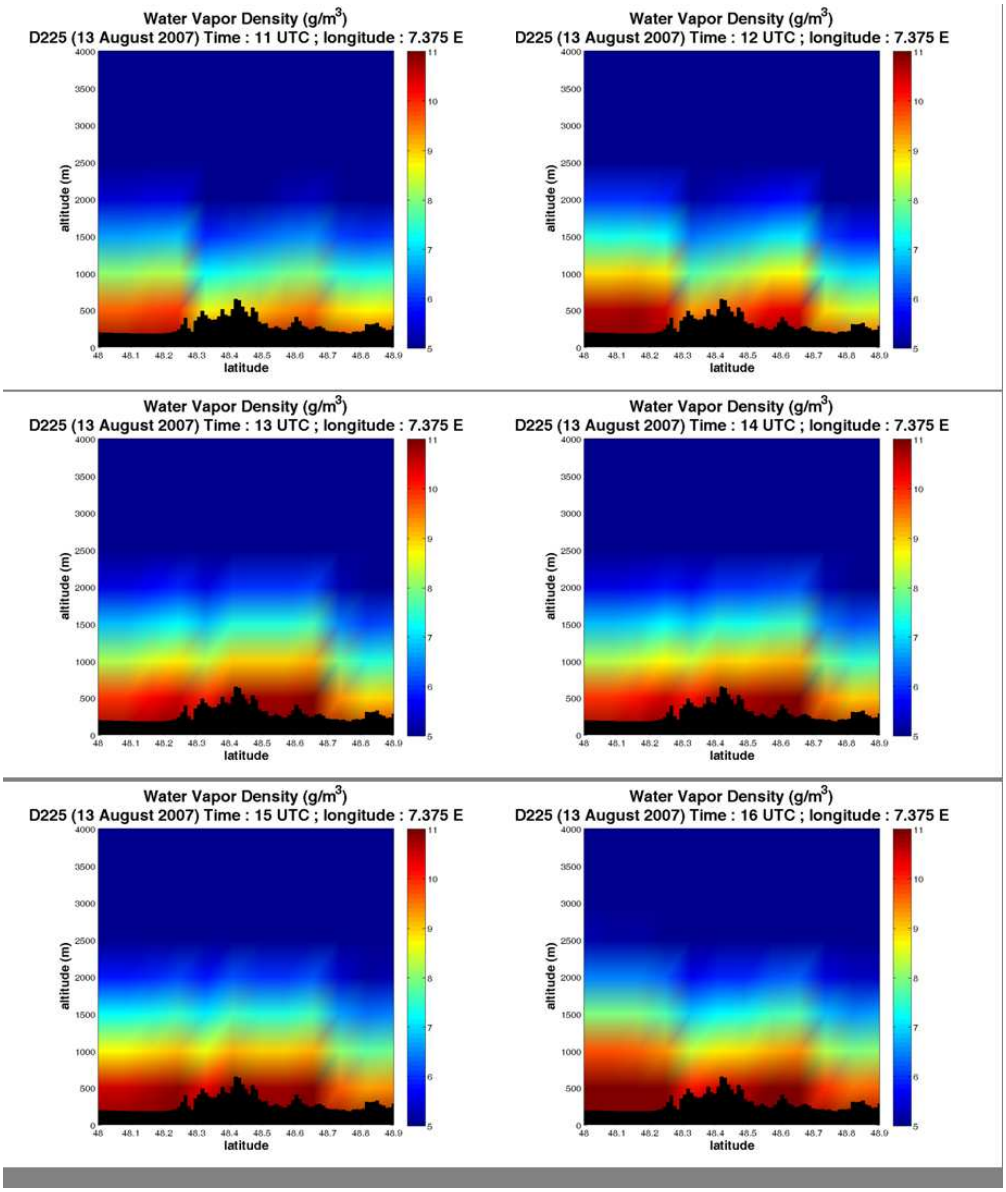

GPS tomography vertical water vapour density cross-sections at constant longitude 7.34° E from 11:00 to 16:00 UTC, on August 13, 2007 (IOP 15b). The water vapour density scale goes from 5 to 11 g/m3.